REPORT DOCUMENTATION PAGE

Form Approved
OMB No. 0704-0188

Public reporting burden for this collection of information is estimated to average 1 hour per response, including the time for reviewing instructions, searching existing data sources, gathering and maintaining the data needed, and completing and reviewing the collection of information. Send comments regarding this burden estimate or any other aspect of this collection of information, including suggestions for reducing this burden, to Washington Headquarters Services, Directorate for Information Operations and Reports, 1215 Jefferson Davis Highway, Suite 1204, Arlington, VA 22202-4302, and to the Office of Management and Budget, Paperwork Reduction Project (0704-0188), Washington, DC 20503.

1. AGENCY USE ONLY (Leave blank)	2. REPORT DATE 16 Apr 96	3. REPORT TYPE AND DATES COVERED Translation

4. TITLE AND SUBTITLE
Laser-Differential Interferometer Applications in Gas Dynamics

5. FUNDING NUMBERS
AFOSR Grant
F49620-94-1-0067

6. AUTHOR(S)
Author: G. Smeets and A. George, I.S.L., France.
Translated by Andreas Goetz, Purdue University

7. PERFORMING ORGANIZATION NAME(S) AND ADDRESS(ES)
Aerosapce Sciences Lab.
3 Purdue University Airport
West Lafayette IN 47906-3371

8. PERFORMING ORGANIZATION REPORT NUMBER

9. SPONSORING/MONITORING AGENCY NAME(S) AND ADDRESS(ES)
Air Force Office of Scientific Research
110 Duncan Avenue
Bolling AFB
Washington DC 20332-0001

10. SPONSORING/MONITORING AGENCY REPORT NUMBER

11. SUPPLEMENTARY NOTES
Translation of Report 28/73, Institute Franco-Allemand de Recherches de Saint-Louis, by G. Smeets and A. George, Nov. 1975. Translated by Mr. Andreas Goetz at Purdue University, School of Aeronautics and Astronautics, March 1996. Translation was corrected by G. Smeets.

12a. DISTRIBUTION/AVAILABILITY STATEMENT
Unclassified unlimited per original source document

12b. DISTRIBUTION CODE

13. ABSTRACT (Maximum 200 words)

The laser-diffferential interferometer described in ISL-T 21/70 and ISL-14/71 underwent further development. It now constitutes a versatile measurement instrument able to be utilized advantageously in the following fields: flow calibration in gas-dynamic facilities, compressible gas dynamics, in particular various types of boundary layers, gas kinetics or chemical kinetics, turbulence investigations, acoustics. The optical arrangements suitable for the respective problems – for the most part already tested – are systematically compiled, and the possibilities of the techniques are demonstrated in a wide variety of examples.

14. SUBJECT TERMS
laser interferometer, gas dynamics, turbulence, laser diagnostics, shock tube

15. NUMBER OF PAGES
67 pages

16. PRICE CODE

17. SECURITY CLASSIFICATION OF REPORT	18. SECURITY CLASSIFICATION OF THIS PAGE	19. SECURITY CLASSIFICATION OF ABSTRACT	20. LIMITATION OF ABSTRACT
UNCLASSIFIED	UNCLASSIFIED	UNCLASSIFIED	UL

NSN 7540-01-280-5500

Standard Form 298 (Rev. 2-89)
Prescribed by ANSI Std. Z39-18
298-102

DTIC QUALITY INSPECTED 1

Dr. G. Smeets - A. George
Deutsch-Französisches Forschungsinstitut Saint-Louis

Institut Franco-Allemand de Recherches de Saint-Louis
5 Rue Du General Cassagnou
68301 Saint-Louis
FRANCE

Report
28/73

Laser-Differential Interferometer Applications
in Gas Dynamics

Saint-Louis
Nov. 7,1973

Chief Engineer   Chairman at the BWB
(Auriol)   (Dr. Schall)

Keywords

Abstract

The laser-differential interferometer described in ISL-T 21/70 and ISL-14/71 underwent further development. It now constitutes a versatile measurement instrument able to be utilized advantageously in the following fields: flow calibration in gas-dynamic facilities, compressible gas dynamics, in particular various types of boundary layers, gas kinetics or chemical kinetics, turbulence investigations, acoustics.

The optical arrangements suitable for the respective problems - for the most part already tested - are systematically compiled, and the possibilities of the technique are demonstrated in a wide variety of examples.

Contents

1. Principles of the Laser-Differential Interferometer

a) Optical Arrangement

The optical arrangement is based on a generic differential interferometer set-up schematic with Wollaston prisms as beam splitters. A continuous gas laser (He-Ne-Laser) serves as a light source, the recording takes place electrically using a photo detector. This results in the basic laser-differential interferometer (LDI) arrangement depicted in fig. 1.

The linearly polarized laser beam emitted by the laser is first circularly polarized by a $\lambda/4$-plate. In a first Wollaston prism, the beam is then split under a small angle ε. The Wollaston prism consists of two cemented partial prisms of a birefringent crystal (Quartz, Calcite). Their optical axes are oriented such that they are normal to each other as well as to the laser beam direction, that is, parallel to the frontal surface of the Wollaston prism. If α is the prism angle and n_{or} and n_{ex} symbolize the ordinary and extraordinary light beam in the crystal, then the division angle ε results from:

$$\varepsilon = 2 \cdot \tan \alpha \cdot \left| n_{ex} - n_{or} \right|. \tag{1}$$

The two partial beams leave the Wollaston prism polarized normally to each other and with a constant phase shift. The phase shift depends on the location, at which the laser beam passes through the Wollaston prism and can be varied arbitrarily by displacing the Wollaston prism perpendicularly to the laser beam.

A lens with focal length f is located at a distance f from the Wollaston prism. In this manner, two parallel partial beams separated from each other by the distance a are generated in the test section, where a is:

$$a = 2f \cdot \tan \alpha \cdot \left| n_{ex} - n_{or} \right|. \tag{2}$$

Usually, the differential interferometer is set up symmetrically. After intersecting the phase object under examination, the partial beams are merged again by a lens of the same focal length and a Wollaston prism of the same type and orientation. The second Wollaston prism changes the phase shift by a constant, adjustable amount. Since the partial beams are still polarized normal to each other, they can generate interferences at the photo diode after intersecting a polarization filter oriented at 45°.

It is of importance to image the phase object on the photo diode by another lens. This is the only way to avoid the effect of laser beam deflection in the phase object on the interference at the photo diode due to refraction index gradients. With this imaging process, the optical path length from the object point to the image point is constant regardless of path variations, according to Fermat's principle.

6

The λ/4-plate will be dispensable, if the laser light is polarized linearly at 45° to the axes of the Wollaston prisms. The usage of a λ/4-plate is very convenient, since the Wollaston prism orientations become independent of the laser and thus arbitrarily variable.

Laser beams of the TEM_{oo}-mode are always employed. The laser power distribution over the beam cross section is then governed by a two-dimensional Gaussian distribution. The optical components, including the sensitive photo diode surface and possible light stops are always larger than the effective beam diameter. In this way any diffraction is avoided.

b) Interference Slope

An ideal interference of two coherent, monochromatic light waves of wavelength λ leads to an illumination intensity E at the photo diode, dependent, as stated in

$$E = E_0 \cdot \cos^2\left[\pi \cdot \frac{\Delta\phi}{\lambda}\right],$$ (3)

on the optical path difference $\Delta\phi$ between the two light beams (Fig. 2). If part of the light does not generate interference (due to unequal intensity of the partial beams or other reasons), a constant illumination $\overline{E}$ independent of $\Delta\phi$ will be superimposed on the interference-dependent illumination E. As long as $\overline{E}$ does not reach the order of magnitude of the amplitude E_0, this will not be relevant for the operation of the laser interferometer. Due to the high degree of focussing, practically all laser energy can be brought to interfere, partial beams generated with equal intensity provided.

The optical path difference $\Delta\phi$ consists of a constant value $\Delta\phi_0$ (given by the Wollaston prism positions) and another part $\delta\phi$ due to the effect of the phase object:

$$\Delta\phi = \Delta\phi_0 + \delta\phi.$$ (4)

In subsequent applications the interferometer is always adjusted to the linear middle part of an interference slope

$$(\frac{\Delta\phi_0}{\lambda} = \frac{1}{4} + \frac{1}{2}n),$$

as shown in figure 2, and provisions are made to ensure that the change in path length $\delta\phi$ produced by the phase object is kept small compared to the light wavelength λ. This can always be achieved by the correct choice of the beam separation a. Then the interference is restricted to the linear part of a slope where the resulting illumination change ΔE is related to $\delta\phi$ by a simple linear equation:

7

$$\frac{|\Delta E|}{E_0} = \pi \cdot \frac{|\delta\phi|}{\lambda}. \qquad (5)$$

c) Signal

For the purpose of signal generation, silicone PIN photo diodes are quite convenient. In the visible range, they achieve a quantum efficiency of 60% to 70%, the time constant is in the range of nanoseconds, and they operate linearly in the whole range of interest. The circuit is outlined in fig.3. It only consists of a power source (battery), the photo diode and a variable resistor. The photo diode operates like a valve by admitting a current proportional to the illumination. Thus, there exists a proportional relationship between the optical path change $\delta\phi$ due to the phase object and the voltage change ΔU at the resistor:

$$\frac{|\Delta U|}{U_0} = \pi \cdot \frac{|\delta\phi|}{\lambda}. \qquad (6)$$

In order to calculate the value of $\delta\phi$ from the signal ΔU, U_0 must be known. U_0 results from the voltage amplitude at the resistor when varying the illumination between its extremal values by displacing one of the Wollaston prisms. By adjusting the resistor, U_0 can be set to a suitable value. If the goal is a high temporal resolution when measuring rapidly changing phase objects, the resistor has to be sufficiently small to ensure a small enough RC-constant in combination with the wire capacitance of the data recording device.

The PIN photo diode 5082-4207 from Hewlett Packard was used. Due to its relatively small detector surface it is insensitive to the room illumination, so that the LDI could be set up without a cover in normally lit rooms.

d) Registration of Unsteady Refractive Index Profiles *n(t)*

The measurement of an unsteady refraction index profile is possible in a simple manner by shielding one of the two partial beams over a length *l*, such that only the other beam is affected by the phase object. The measured optical path change $\delta\phi$ is then related to the instantaneous refractive index *n(t)* by

$$\delta\phi(t) = l \cdot \left[n(t) - n_0 \right]. \qquad (7)$$

The refractive index before the advent of the phase object is n_0.

Figure 4 shows, for example, the registration of an unsteady density profile of a hypersonic flow in the test section of a shock tube. One of the laser beams was shielded from the flow by a small tube of 1 cm in diameter and 10 cm length. The tube was closed by glass windows and featured sharpened rings on both ends in order to prevent gas from the stagnation regionto

pass in front of the window. The recording shows that after the starting time the flow maintained a constant density of approximately $3 \cdot 10^{-3} \, \rho_N$ for about 200 μs.

Similarly, the density profile in a pressure wave can be measured. In this case it is appropriate to shield the laser beam by a thin capillary to avoid disturbance of the measured density as much as possible.

For measurements in the shock tube, a rectangular cross section is well suited. Then one of the laser beams can simply be sent through an orifice in the side wall. Figure 5 shows the measurement of the density profile between the shock wave and the contact surface.

To avoid a boundary layer effect on these measurements of the density profile behind the incident or reflected shock wave, a test section with slanted windows can be used (fig. 6). The slant angle of the windows can be achieved in a shock tube with triangular or trapezoid cross section, or in a circular cross section by eccentric mounting of the windows. Both beams can then be sent through the same window boundary layers, so that the optical path difference is not affected by the density changes in the boundary layers. This of course is only valid as long as the boundary layers remain laminar and undisturbed. The measurement effect comes as a result of the different geometrical paths of the partial beams in the flow. With a test section window slant angle β and a beam separation a, the relationship between the measured optical path change $\delta\phi$ and the instantaneous refraction index $n(t)$ (symmetrical intersection assumed) is

$$\delta\phi(t) = 2a \cdot \tan\frac{\beta}{2} \cdot \left[n(t) - n_0\right] = a \cdot \beta \cdot \left[n(t) - n_0\right]. \qquad (8)$$

2. Laser-Differential Interferometer Sensitivity

a) Quantum Noise

For the registration of single events, the sensitivity limit is given by a signal-to-noise ratio of 1. There are several types of noise, or voltage disturbances, where photon or quantum noise constitutes the principal limit of the attainable sensitivity.

With a laser output in the mW-range, the photo diode current lies in the mA-range. Then the signal-to-noise ratio

$$\frac{S}{N} = \frac{I}{\sqrt{2 \cdot e \cdot I \cdot \Delta f}} \qquad (9)$$

is greater than 10^5 at $\Delta f = 100$ kHz, and still greater than 10^4 at 10 MHz. Compared to this, the working resistance noise is negligible.

b) Compensation of Laserlight Fluctuations

The light from every continuous laser possesses a more or less strong amplitude fluctuation. For good lasers, this fluctuation is in the order of magnitude of 1/1000. However, it already leads to a substantial decrease of the signal-to-noise ratio compared to the theoretically achievable value. Figure 7 shows an optical arrangement compensating to a great extent for these "coherent" laserlight fluctuations.

In this arrangement, a combination of a $\lambda/4$-plate and an additional Wollaston prism replaces the polarization filter. Then at the same instant, two interferences on two separate diodes shifted in phase against each other by π are created, and thus rest on opposite interference slopes. The difference between the two signal currents is generated electrically. This is being accomplished either by a difference amplifier or simply, as shown in figure 7, by sending the currents in opposite directions through the working resistor. By generating the difference, small disturbances due to laserlight fluctuations are largely suppressed, whereas the signal voltages proportional to optical path changes add up.

Using this method, it is possible to measure in a frequency range between 100 Hz to 10 MHz with a signal-to-noise ratio greater than 10^4, such that according to eqns. (5) or (6) optical path changes of $\lambda/30,000$ and less can still be recorded. At the upper frequency limit above 10 MHz, the sensitivity is restricted by quantum noise. In the low frequency region, disturbances due to air turbulences, vibrations and infrasound can occur and diminish the signal-to-noise ratio.

c) Vibration Compensation

Due to the small beam separation distance an LDI possesses a comparatively small vibration sensitivity. With little effort, the adjustment to the middle of a slope can be retained over a prolonged period of time. However, in the case of very sensitive measurements, minimal vibrations (possibly generated by the phenomenon itself) can lead to substantial disturbances.

Using the arrangement outlined in fig. 8 in those cases can achieve compensation of the most part of vibration-induced disturbances. Here, the laser beam is divided by an additional Wollaston prism into two beams before entering the actual interferometer. A $\lambda/4$-plate gives circular light beam polarization. The dividing Wollaston prism is imaged to the first interferometer Wollaston prism by a lens. Two beam pairs come into being in the test section, of which - if possible - only one is sent through the phase object. The beam pairs interfere on separate receivers. The differential interferometer can be adjusted such, that both interferences lie on the same slope and mechanical vibrations lead to in-phase signal disturbances. By subtracting the signals from each other using the circuit in fig. 7, the noise due to vibrations and due to laserlight fluctuations can be suppressed simultaneously.

10

d) Registration of a Sound Wave

Figure 9 shows the signal of a sound wave as an example for the high attainable LDI sensitivity. One of the laser beams was protected against the sonic field by a thin capillary about 10 cm long. The signal was generated by tapping against a door.

These sound waves are very weak phase objects. A pressure gradient Δp in standard atmosphere with a shielded length of $l = 10$ cm leads to an optical path change $\delta\phi$ as expressed in:

$$\frac{\delta\phi}{\Delta p} = 2.1 \cdot 10^{-3} \, cm \, / \, bar \qquad (10)$$

A sonic wave amplitude in the μbar-range (about equivalent to 70 dB) causes optical path changes smaller than 1 Å. In the example demonstrated here, a resolution of 0.1 Å or $\lambda/60,000$ was achieved.

3. Spatial Resolution

a) Focussing of Laser Beams

The intensity I of an ideal laser light bundle (TEM_{oo}) is governed by the following distribution function:

$$I(r,z,\vartheta) = \frac{8 \cdot P}{\pi \left[(z\vartheta)^2 + \left(\frac{4\lambda}{\pi\vartheta} \right)^2 \right]} \cdot \exp\left\{ -\frac{8r^2}{(z\vartheta)^2 + \left(\frac{4\lambda}{\pi\vartheta} \right)^2} \right\}. \qquad (11)$$

P designates the laser output power, r the distance from the bundle axis, z the distance to the focal plane and ϑ the divergence angle of the bundle. Over the bundle cross section ($z = $ const.), the beam intensity varies with a Gaussian distribution:

$$I = I_0 \cdot \exp\left\{ -\frac{2r^2}{r_0^2} \right\}. \qquad (12)$$

The radius r_0 denotes the beam bundle boundary. At this location, I has dropped by the factor $1/e^2$ compared the maximum value I_0 (see figure 10). The bundle divergence angle ϑ is also measured at this bundle "boundary". The laser bundle diameter d is then:

11

$$d = 2r_0 = \sqrt{(z\vartheta)^2 + \left(\frac{4\lambda}{\pi\vartheta}\right)^2} \ . \tag{13}$$

At the focal plane ($z = 0$) it reaches its minimum value $\hat{d}$:

$$\hat{d} = \frac{4\lambda}{\pi\vartheta} \ , \tag{14}$$

which depends on the divergence angle ϑ.

In order to achieve high spatial resolution with the LDI, it is not sufficient in most cases to concentrate the laserlight on a very small diameter $\hat{d}$ by choosing a wide bundle divergence angle ϑ. For most applications it is necessary to confine the light in a diameter as small as possible over a given distance l.

The volume V occupied by the laserlight over the measurement distance l (when focussing in the middle of the measurement distance) is:

$$V = 2\int_0^{l/2} \frac{\pi}{4} d^2 dz = \frac{\pi}{48} \cdot \vartheta^2 l^3 + \frac{4\lambda^2 l}{\pi\vartheta^2} \ . \tag{15}$$

It reaches its minimum value with a bundle divergence angle:

$$\vartheta^* = \sqrt{\sqrt{3} \frac{8}{\pi} \frac{\lambda}{l}} = 2.1 \cdot \sqrt{\frac{\lambda}{l}} \ . \tag{16}$$

Then the bundle diameter in the focal plane is:

$$\hat{d}^* = \sqrt{\frac{2}{\pi\sqrt{3}} \lambda \cdot l} = 0.61\sqrt{\lambda \cdot l} \ . \tag{17}$$

The maximum diameter at the ends of the measurement distance ($z = l/2$) is:

$$\hat{d}^*_{max} = \sqrt{\frac{8}{\pi\sqrt{3}} \lambda \cdot l} = 1.21\sqrt{\lambda \cdot l} \ , \tag{18}$$

and the mean value of d^* is:

$$\bar{d}^* = \sqrt{\frac{4}{\pi\sqrt{3}} \lambda \cdot l} = 0.86\sqrt{\lambda \cdot l} \ . \tag{19}$$

12

Figure 11 depicts an arrangement, by which focussing the laser bundle in the test section can be achieved. First, the laser beam is widened by a lens with short focal length and then focussed in the test section by means of a second lens. When correctly choosing the focal lengths and the arrangement of the two lenses, the desired divergence angle ϑ as well as the focal point position in the test section can be realized.

A very simple relation between ϑ and the laser bundle diameter D in the first Wollaston prism exists:

$$D = \vartheta \cdot f \qquad (20)$$

This relationship is independent of the focal point location in the test section. In order to find the desired focussing conditions (realization of ϑ, $\hat{d}$ or ϑ^*, $\hat{d}^*$ respectively), this easily controllable parameter D serves the purpose.

b) Focussing using Cylindrical Lenses

When replacing the two focussing lenses in fig. 11 by corresponding cylindrical lenses, focussation in only one direction results. In the other direction, the laserlight bundle can also be formed independently by cylindrical lenses. E.g., when placing a cylindrical lens with a very small focal length in front of the first Wollaston prism at the distance of this focal length, then wide light bands are generated in the test section. The measurement with those light bands results in averaging in one coordinate direction and a simultaneous high spatial resolution in the other.

c) Measurement of a Shock Front Profile

The density jump in a shock front takes places within a few mean free path lengths. Therefore, the registration of the density profile during transition through a shock wave requires high spatial and temporal resolution.

For the measurements, the optical arrangement in fig. 8 with two beam pairs was employed. The beams were adjusted exactly parallel to the shock front and were focussed in the middle of the test section on a diameter of $\hat{d} \approx 0.1$ mm. They were shielded by capillaries of 10 mm and 48 mm length and an inner diameter of 1 mm (see fig. 12). The end effects on the capillaries affect all beams in the same manner and generate no contribution to the signal. The recorded optical path change increases proportional to the density due to the differing shield lengths. The diode circuit was set up with low capacitance and resistance to create a bandwidth of about 20 Mhz.

13

4. Multiple Beam Arrangements

a) Beam Multiplication with Wollaston Prisms

To increase the amount of spatial information, the LDI can be set up to measure with several beam pairs simultaneously. Fig. 8 already showed how to achieve conveniently a beam duplication with an additional Wollaston prism and a λ/4-plate. With several Wollaston prisms and λ/4-plates many beams can be generated at the same time (fig. 13). When decrementing the prism angles stepwise by a factor of 2 and imaging the set of prisms into the first Wollaston prism with a lens, parallel and equidistant beam pairs are produced in the test section.

b) Registration with Multiple Diode Arrays

For simultaneous registration of the interference signals from many beams, diode arrays are quite convenient. The diodes are regularly spaced in a stripe-like arrangement. Figure 14 gives the diode circuitry. The individual circuits share a common power source and have a variable working resistor each, on which the voltage signals can be picked off.

Up to the present the LDI has been operated with 8 beam pairs. This number can easily be increased, when providing the appropriate number of registration channels.

c) Density Profile of the Laminar Shock Boundary Layer

The signals in figure 15 resulted from by 8 adjacent laser beams crossing a laminar shock boundary layer. Such a boundary layer builds up when a shock passes over a model of finite length. It is unsteady at first, but after some time converts into the steady boundary layer on the model.

The second beam of each beam pair is located outside the boundary layer (not drawn in fig. 15). Thus, each signal represents the instantaneous optical path increase of the respective laser beam in the boundary layer at any moment in time. All signals together represent the optical path profile of the boundary layer as a function of time.

The model was a hollow cylinder of 3 cm diameter with its axis parallel to the propagation direction of the shock wave. Due to the axisymmetry of the observed boundary layer (on the outer surface of the cylinder), the density profiles of the laminar boundary layer can be gained from the measured optical path profiles by applying an Abel inversion. The laser beams were focussed on a minimal diameter of $\hat{d} = 0.05$ mm. Thus the less than 1 mm thick boundary layer can already be resolved well.

d) Time-Averaged Density Profiles of Turbulent Flows

At higher densities and Reynolds numbers, the boundary layer became turbulent shortly after the transition of the shock wave. Figure 16 displays the signals from such a turbulent shock boundary layer. Here the beams of each pair are separated by only 0.125 mm and thus share one beam. Then the optical path lengths of the inner beams result from the sum of the signals from the beams located further out.

The laser beams were focussed still better - to a few hundredths of a Millimeter - in order to resolve this boundary layer.

The signals reveal immediately, that the boundary layer directly behind the shock front is still very thin and laminar, since during the first 30 µs after the passing of shock wave only the signal from the innermost beam pair shows an increase while still being free of the oscillations indicative of boundary layer turbulence.

With the same LDI set-up density profiles of a heated, turbulent, axisymmetric, subsonic free flow were also measured. In this case, the fluctuating part of the signals caused by turbulence was even far greater than their time-averaged mean values. In spite of this, a fairly precise determination of the time-averaged density profiles was possible without difficulties.

e) Density Profiles of Hypersonic Flow around Cones

The signals in fig. 17 stem from the flow field around a blunt cone in a hypersonic flow field of Mach number M = 9. The flow was generated in a shock tube with nozzle expansion and consists of an unsteady initial flow during the starting phase of the nozzle and a steady flow phase with a duration of about 200 µs. Again, the measurements took place using 8 beam pairs, of which only one beam each is sent through the flow field between bow shock and cone. From the signals the optical path profile during the period of steady flow can be gained, and can then be converted to the respective density profile by applying an Abel inversion. Since in a strict sense the Abel inversion requires axisymmetry of the flow field, it was assumed that the flow sector seen by the laser beams on the forward side of the slightly incidented cone can be approximated as axisymmetric. The beams were focussed to $\hat{d} = 0.04$ mm.

f) End Wall Boundary Layer in a Shock Tube

After the normal reflection of a strong shock wave at the end of a shock tube the gas is heated up strongly. At the end wall, a temperature boundary layer is generated.

Fig. 18 displays signals from this boundary layer. The beam separation of the 4 laser beam pairs was extremely small - $a = 0.07$ mm - such that the signals were proportional to the

15

density gradient. With regard to the test section width $l = 10$ cm (shock tube diameter), the beams were focussed on $\overline{d} = 0.2$ mm.

The signals show how the boundary layer grows over time. A quantitative analysis permits the determination of the thermal diffusivity $\lambda/\rho c_p$ and with known c_p the thermal conductivity λ of the high temperature gas.

5. Profile Measurements using Deflecting Mirror

a) Arrangement with Deflecting Mirror

By turning a small mirror, the laser beams can be parallely displaced in the test section, such that within a certain time they cross the phase object. The optical path profile of objects that do not change during this time (e.g. steady boundary layers) can be measured in this manner. Fig. 19 shows a suitable optical arrangement. The laser beam is incident on a small deflecting mirror (if necessary after being sent through a lens for the adjustment of the beam diameter at the mirror location). The mirror is imaged by another lens into the first Wollaston prism of the interferometer. Rotating the mirror then leads to a parallel displacement of the beams in the test section.

In absence of a phase object, the beam displacement must not cause a signal. To fulfill this, some prerequisites have to be met. All optical components have to be clean, that is, there must be no local absorption. The interferometer components must possess high optical quality in order to be able to adjust the interferometer to the same point on a interference slope over the whole region crossed. Even with high-quality components, the latter condition can only be met with sufficiently small beam separation. Then the signals give the gradients of the optical paths. For this reason, the method is not suitable for highly sensitive measurements on weak phase objects.

In order to measure the profile, the deflecting mirror receives the same sawtooth voltage function that serves as the time basis of the recording oscilloscope. Then the profile appears directly on the oscilloscope screen. Deflecting mirrors able to follow frequencies of up to 10 kHz are available. Using these, profile measurements in 100 µs are possible.

b) Density Profile of a Temperature Boundary Layer

As an example of a profile measurement using a deflecting mirror, fig. 20 shows the profile of a heated vertical flat plate. Here, the beam separation distance was only about 1/10 mm. Since the phase object is flat - the plate was adjusted parallel to the laser beams - the signal is proportional to the density gradient. The signal was written within 2 ms. During this time, the laser beams were parallely displaced by about 1 cm with uniform velocity.

6. Electronic Signal Integration

a) Circuitry

It is easily possible to integrate the signals recorded with the aid of the deflecting mirror electrically and so to obtain the optical path profile of the phase object directly instead of the gradient profile. The integration can take place by means of the circuit shown in fig. 21. Instead of the additional RC-element responsible for the integration, one can also use an internal RC-element of an ocsilloscope plug-in unit with adjustable upper bandwidth limit.

The optical path profile $\phi(y)$ is given by:

$$\left|\phi(y) - \phi_0\right| = \frac{1}{\pi} \frac{\lambda}{a} w R_2 C \frac{|\Delta U_i|}{U_0},$$

(21)

where ϕ_0 is the optical path outside the phase object, a the beam separation distance (here oriented in the direction of beam deflection), and w the deflection speed of the laser beams in the object. ΔU_i is the integrated signal, U_0 has the same meaning as in eqn. (6), which is the voltage amplitude at the working resistor R_1 when varying the illumination intensity at the photo diode between its extremal values by displacing the Wollaston prism. For the derivation of equation (21), $R_2 \gg R_1$ was assumed.

For the recording of the profiles it is useful to have the laser beams pass from the undisturbed region into the phase object, that is, to begin the integration from the boundary.

b) Integrated Temperature Boundary Layer Profile

The density gradient profile of the temperature boundary layer in fig. 20 was integrated electrically in the manner described. The integrated signal constitutes the density profile. From this, the temperature profile can be calculated immediately.

c) Integrated Signals from Moving Phase Objects

For direct integration, gradient signals from phase objects in motion are suitable as well. If the phase object crosses the laser beams with a constant velocity w and does not change its shape, eqn. (21) can be employed for the calculation of the optical path profile $\phi(t)$ in this case also. The laser beam deflection is unnecessary, likewise the experimental effort (high-quality optics) associated with it. The beams also have to be separated in the direction of motion of the phase object in order to measure the gradient in the direction of the motion.

17

Moving phase objects of this kind are - among others - propagating pressure waves and shock waves and their relaxation regions. In fig. 22, the gradient signal and the integrated signal of a sound wave are presented.

The wave was produced by a high-frequency loudspeaker and a square impulse. Due to the discontinuous displacement of the loudspeaker membrane an N-shaped wave (steep pressure wave with a successive decay to a negative pressure) is generated. Furthermore, the loudspeaker appears to be excited with an eigenfrequency.

At a sufficiently large distance from the loudspeaker, the wave can be regarded as constant in shape and within the unprotected region of the laser beams as plane. The integrated signal then gives the exact sound wave density profile. By this method it is possible to determine the characteristics of electroacoustic transmitters directly.

d) Laser-Differential Interferometer used as a Microphone

Sound waves are extremely weak phase objects. As already explained in chap. 2d, an LDI can therefore serve only as a very insensitive microphone. However, an interesting field of application opens up in the area of strong sound waves, especially of ultrasonic waves. There, the LDI can gain decisive advantages compared to other microphones. Since the density function of a planar wave can be determined quantitatively, the LDI would represent an ideal calibration microphone with no restrictions in frequency response. A feedback from the microphone to the measured sound wave is also avoidable. Difficulties arise at low frequencies, since an LDI with the high sensitivity necessary for sound measurements is highly prone to be disturbed by mechanical vibrations and temperature turbulences. Such disturbances are dominant in the frequency range below 20 Hz.

Fig. 23 shows a possibility to assemble a directionally selective microphone with enhanced sensitivity. The bundled dual beam from the LDI is being folded between two mirror surfaces by multiple reflection. The total beam path can easily exceed 10 m. A gradient-sensitive plane is being built up to register normally incident planar sound waves. The mirror surfaces can be designed as two thin stripes in order to minimize disturbances of the sound field. These have to be connected to each other by rigid beams, since displacement of the mirrors with respect to each other would cause strong signal perturbations. On the other hand, displacement of the frame as a whole does not cause problems. The frame, which is the actual microphone, can be set up remote from the rest of the optics.

This directional microphone is intended to be utilized in the near future for the detection of sound waves in turbulent free flow. For this purpose, the system is combined with a parabolic reflector as shown in fig. 24. When adjusting the sensitive surface normally to the paraboloid's axis of symmetry, only those sound waves that are emitted in the focal point of the paraboloid and radiate from there as spherical waves are registered with high sensitivity. Preliminary tests showed that this system performs as expected. Using a small nozzle on a pressurized air hose, ultrasonic sound waves were generated, which, when emitted in the focal point of the

18

paraboloid, lead to substantial signals. The magnitude was highly dependent on the nozzle exit position. At just a little distance from the focal point, the signals immediately grew weaker by an order of magnitude.

7. Strong Phase Objects

a) Reduction of Beam Separation

Until now, it was assumed that the optical path change $\delta\phi$ caused by the phase object remains small compared to the laser wavelength λ. The linear relationship (6) between $\delta\phi$ and the resulting signal ΔU is only sufficiently valid for $\delta\phi \leq 0.15\lambda$. In the intervall $\delta\phi \leq 0.4\lambda$ there is still a unique but nonlinear relation between $\delta\phi$ and ΔU. Still greater amplitudes of optical path change would lead to overshooting and thus are not permissible in the operational mode chosen until now.

However, by reducing the beam separation a the sensitivity of the interferometer can arbitrarily be decreased (there is no lower limit for a), such that in principle the condition $\delta\phi \leq 0.15\lambda$ can be fulfilled with strong phase objects as well. The LDI then gives optical path gradients which can be integrated in many cases in the manner described above.

b) Interference Stabilization using a Deflecting Mirror

A very different method to enhance the measurement range significantly exists. The principle is demonstrated in fig. 25. The laser beam is sent through two successive differential interferometers. The phase object is located in the first one as usual. The second interferometer is arranged with a beam path reflected by a small deflecting mirror. Between both interferometers a small lens is located if needed. The phase object is imaged onto the deflecting mirror and the latter onto the photo diodes. Rotating the mirror displaces the laser beams in the Wollaston prism of the second interferometer. This causes an additional optical path difference $\Delta\phi^*$ proportional to the mirror rotation angle β. The relation is:

$$\Delta\phi^* = \frac{1}{2}\beta \cdot a. \tag{22}$$

A control circuit controls the current through the coil vibrator and thus the mirror position, such that the signal difference of the two diode circuits is always zero. The optical path change in the phase object is then compensated instantly by a corresponding mirror rotation. The mirror rotation angle, i.e. the related control current change is proportional to the optical path change and can be recorded as a measure of the latter.

This method will also be applicable, if the optical path change in the phase object measures many wavelengths. The only limit exists with respect to the rate of change of the phase object.

19

Due to the mechanical inertia of the mirror deflection systems, changes can only be detected with a frequency bandwidth ≤ 10 kHz. The system does not follow changes faster than this anymore, and is moreover prone to jump to another interference slope.

c) Interference Stabilization using a Pockel Cell

Instead of a deflecting mirror, a Pockel cell can serve to generate an additional optical path difference. The arrangement is depicted in fig. 26. The voltage on the Pockel cell can be adjusted here as well, such that the signal difference at the diodes vanishes. Then the control voltage is again proportional to the path change in the phase object.

When using a Pockel cell, the control loop can follow rapid changes as well. In this case, however, the amplitudes may not be too big, since high voltages are necessary for the Pockel cell control and high-voltage amplifiers with sufficient bandwidth do not exist.

The interference control loop can also be employed for compensating strong LDI hardware vibrations. When designing the control loop such that it can only follow up on low frequencies (< 50 Hz) prevalent in vibrations of the optical hardware, it can compensate their effects. The interferometer adjustment to the middle of a slope remains. Optical path changes due to the phase object shorter in time than 1 ms (short duration events) do not affect the control loop and can be registered in the usual way.

d) Interference Stabilization by Displacement of a Wollaston Prism

Of course, the simplest method of interference compensation is displacing one of the two Wollaston prisms normal to the optical axis. Due to the comparatively large Wollaston prism masses they can only follow up on relatively low frequencies. An estimation reveals, that by using magnetic coils the Wollaston prisms can be displaced with frequencies up to about 100 Hz. This is sufficient to achieve compensation of strong LDI set-up vibrations.

Since the PIN-diodes work like valves for the electric current, they open the possibility to use the simple control loop shown in fig. 27 for interference stabilization. The capacitor C is connected to the input of a charge amplifier. The output dictates the current through the coil vibrator of the deflecting mirror or the Wollaston prism, or the Pockel cell voltage respectively. The control function is based on the inequality of the currents through the photo diodes with an interference deviating from the middle of the interference slope. Then the capacitor C changes its charge and voltage and thereby shifts the interference back to the middle of the slope.

The resistor R in the circuit is necessary only when compensating for mechanical vibrations to generate a slow response with a large RC constant. The signals of the short duration events to be recorded can be picked up at the resistor R.

To obtain a fast response, the resistor R is shortened out. In this case, the voltage at the capacitor C is the measured signal proportional to the optical path change in the phase object.

8. Laser Light Bundles with large Diameter

a) Beams through Turbulent Test Section Window Boundary Layers

At higher densities of the flow, the boundary layers at the test section windows of shock tubes or wind tunnels become turbulent. The LDI beams have to be sent through these boundary layers. The expected disturbances can be strongly diminished by choosing great beam divergence angles and focussing in the phase object between the windows at the same time (fig. 28). The beams then overlay each other in the window boundary layers and have large diameters, such that the laser power is distributed over a large number of incoherent turbulent eddies.

On the other hand, with increasing divergence angle ϑ the spatial resolution decreases for a given phase object of dimension l. When focussing in the middle of the phase object, the bundle diameter at the edge of the object reaches the value (also see eqn. (13), where $\lambda = 0$, $z = l/2$):

$$d = \frac{1}{2} l \cdot \vartheta \tag{23}$$

For the measurement of density profiles of the turbulent shock layer (fig. 16), $\vartheta = 0.06$ was chosen as a compromise. The shock tube diameter measured 10 cm. Therefore, the laser bundles at the test section windows measured 3 mm in diameter. The extension of the phase object l measured only a few mm (length of the light paths in the axisymmetric turbulent boundary layer of only several tenths of mm thickness). Thus the spatial resolution was about 1/10 mm.

b) Local Turbulence Measurements

The usage of extremly large bundle angles leads to "local" measurements of fine-structured turbulences. This is explained by fig. 29. Here, the beam separation is small enough to have the partial bundles overlap nearly completely. The bundle drawn in can be perceived as a band of double beams, of which each measures the optical path gradient along its path and contributes equally to the total signal at the photo diode. In the vicinity of the focal point all beams are affected by the same gradient. With increasing distance from the focal point the bundle cross-sectional diameter increases rapidly and includes an increasing number of incoherently changing turbulent regions. Their contributions to the final signal add up and loose influence. It can be shown that the registered signal largely stems from the turbulence region, where the fluctuations are strongly correlated over the entire bundle cross section.

It was possible to operate the LDI with bundle divergence angles of up to $\vartheta = 0.4$. By duplicating the system, simultaneous measurements and thus correlation measurements can be performed at two adjacent points. Fig. 30 shows an optical arrangement employed for this purpose. The laser beam is converted into a highly divergent bundle by a microscope objective. A Koester prism behind it causes the duplication of the bundle. Thus, 2 light bundles with parallel axes, which can be focussed on adjacent locations in a turbulent object are generated. Due to the Wollaston prism effect, the light beams comprising the bundle are gradient sensitive double beams with very small beam separation. In order to compensate for the laser noise, the signal difference is again generated.

The highly focussed LDI was tested for the first time within a heated, turbulent subsonic free flow, as sketched in fig. 30. The flow boundary exhibits strong density fluctuations, whereas the core of the flow is affected by a substantially smaller level of turbulence. Fig. 31 shows a measured fluctuation profile at varying distances y between bundle axis and free flow axis while focussing in the plane of symmetry of the axisymmetric flow. For comparison, the fluctuation profile measured with an LDI without focussing the beams also shown. The comparison clearly reveals the "localizing" effect of strong focussing. When e.g. focussing on the free flow axis, the measured mean squared fluctuation U^{*2} becomes very small in spite of the beams of the laser bundle crossing the turbulent boundary of the free flow.

Although for the main part the signals are generated in the neighbourhood of the focal point, it is not directly possible to conclude from the measured effective signal fluctuations on the effective values of local density fluctuations, i.e. density gradient fluctuations. The relation between signal and density fluctuations is rather governed by the turbulence structure, which first has to be determined by extensive correlation measurements. But this means that at all locations in the free flow cross section of interest the correlation lengths on the three principal axes have to be determined.

The determination of the effective values of the local density fluctuations in the general case of inhomogeneous, anisotropic turbulence requires - as it turned out - substantial experimental effort. Moreover, in this case it cannot yield very precise results, since in the course of the data reduction some simplifying assumptions have to be made. The method is still meaningfully applicable where extreme conditions (high flow velocities, temperatures, fluctuation frequencies, impure flow) preclude any other preciser and simpler measurement methods.

On the other hand, it is possible to determine the spectral distributions of the density fluctuations, and the drift velocity and lifespan of individual turbulences (eddies) by space-time correlations without major difficulties.

c) Reflection in the Focal Point

For correlation measurements in turbulent boundary layers, an arrangement as shown in fig. 32 is suitable as well. The laser light bundle is focussed in the boundary layer and is

reflected back from the mirror-like model surface. Again, the major characteristic of the beam path is very small beam separation at a very large bundle divergence angle. Then, the reflecting surface does not need to possess any special optical quality. It only has to be reasonably smooth and must not destroy the laser light bundle coherence. In the boundary layer on the test section window the laser bundle has a large cross-sectional diameter, such that its contribution to the signal is small. In order to measure correlations, this system can easily be duplicated as well.

d) Local Detection of Sound Waves

The same beam path as in fig. 29 or fig. 30 respectively was used to detect sound waves in the shock tube, which are radiated from a turbulent boundary layer in a supersonic flow. For this, the same hollow cylinder, at which the density profiles of laminar and turbulent shock layers had been investigated before, was reinstalled in the shock tube. The laser light bundles ran outside the turbulent boundary layer on the model and were focussed in the vicinity of the model surface in order to record ultrasonic waves radiated from there. Because of their large divergence angle, the laser bundles became insensitive to the sound of short wavelength at some distance from the focal points. With this arrangement, the noise level due to the sound radiated from the turbulent shock tube boundary layers was largely suppressed.

The signals gained were sent through extreme high-pass filters and amplified to the quantum noise limit. In the upper half, fig. 33 shows a pair of signals indicating the acoustic waves. By extreme focussing and filtering, the strong disturbances from the turbulent flow phenomena of the window boundary layers, which cause a hundred-fold stronger optical effect, could be suppressed except for a minor wavyness of the signal trace. For comparison, the third signal was recorded in absence of the hollow cylinder. The lower signal was registered without flow and shows the measurement noise. It can be seen, that here the maximum LDI sensitivity, by which optical path changes of about 0.1 Å can still be detected, was exploited.

In a further experiment with the aid of the LDI featuring strong focussation, an attempt will be made to measure precisely the profile of flow speed and of the speed of sound vs. time behind the shock wave in a shock tube. Two laser bundles will be focussed on two different locations on the shock tube axis and thereby indicate the arrival of a series of weak spark burst waves generated upstream with a small spark generator in the tube wall.

e) Measurement of Density Profiles behind Shock Waves

Measurements of density profiles in shock tubes are always affected by the boundary layers on the test section windows, through which such measurements necessarily have to be conducted. The effects of a laminar and undisturbed boundary layer can, as explained in chap. 1d, be largely canceled by using slanted test section windows. However, this will be impossible, if the boundary layers are heavily disturbed by the transition between the circular shock tube cross section and the planar windows, or if the boundary layers are turbulent.

In those cases, the signals can be improved by making use of the full window opening and setting up the LDI with correspondingly large bundle diameters. If a high spatial or temporal resolution of the (one-dimensional) density profile is required, cylindrical Lenses can generate a band of light that at least allows full use of the window height.

Determination of refractive index or density profiles is also possible in higher density regions, if the boundary layers in the shock tube are turbulent. By choosing a suitably small beam separation distance a, the optical path changes can always be kept below $\lambda/10$ even at large refraction index changes, such that according to eqns. (6) and (8) the unique relation and proportionality between the signal and the refractive index change is maintained.

9. Self-luminous Phase Objects

a) Filters and Light Stops

With increasing temperature, gases begin to glow. When measuring such phase objects, it is necessary to keep the radiated light away from the LDI photo diodes. A system consisting, as shown in fig. 34, of two light stops and an interference filter serves the purpose by fully passing the laser beam, but for the most part filtering the illumination from the object. The intensity permitted by the system solely depends on the spectral illumination density in the laser wavelength range. The laser is a light source of extremely high illumination density and exceeds all conventional light sources by several orders of magnitude in this respect.

However, experiments on self-luminous phase objects shielded by a light stop/filter system have to fulfill the requirement, that the absorption inherent in all emissions does not cause a noticeable weakening of the laser light intensity.

b) Laserlight Absorption

The effect of a weak absorption of laser light in the object on the signal can be offset by the compensation method (fig. 7).

If the level of absorption increases, the intensity of each of the partial beams has to be measured separately after intersecting the phase object. This can take place by means of the arrangement shown in fig. 35, where a partial mirror deflects the beams before their merging in the second Wollaston prism and sends them to two photo diodes. The simultaneous, separate measurement of the beam intensities I_1, I_2, and that of the interference I allows to determine the optical path difference $\Delta\phi$. The relationship is:

$$I = I_1 + I_2 + 2 \cdot \sqrt{I_1 I_2} \cos(2\pi \frac{\Delta\phi}{\lambda}). \tag{24}$$

10. Dual Wave Length Laser-Differential Interferometer

The principle of dual wavelength interferometry can also be put into practice with the LDI. Thus, sensitive measurements of electron density profiles become possible. The advantage over measurements with microwaves consists of the substantially better spatial resolution.

Electrons give a negative contribution to the refractive index, which is proportional to the electron density n_e and to the square of the light wavelength λ:

$$n - 1 = -4.5 \cdot 10^{-14} \lambda^2 \cdot n_e \qquad (25)$$

where n_e is to be inserted in particles/cm^3 and λ in cm. At the LDI's upper resolution limit of 0.1 Å, refractive index changes of 10^{-10} can be detected with a measurement length of $l = 10$ cm. At the laser wavelength of $\lambda = 6328$ Å, this is equivalent to an electron density of $n_e = 5.6 \cdot 10^{11}$ cm^{-3}.

The optical components of the LDI (Lenses, Wollaston prisms of quartz and calcite respectively) are useable in the wavelength range 0.4 $\mu \leq \lambda \leq 2$ μ, when using quartz lenses, even from 0.3 μ upward. A second wavelength $\lambda = 1.15$ μ in the near infrared is offered by the He-Ne-laser. The registration can take place using suitable germanium detectors (S14).

11. Fields of Application

The table in fig. 36 compiles the main fields of application for the LDI as deducted from experiences in the field of gas dynamics up to the present.

Figures pertaining this report and eventual earlier reports or publications about the respective investigations are also listed in the table.

12. Details about the Laser-Differential Interferometer Components

Laser:
HeNe-laser were exclusively employed, in particular the lasers from Spectra-Physics Mod. 120 (5 mW) and Mod. 124A (15 mW) and a laser from CW-Radiation Model S405R (5 mW). All three lasers emit a linearly polarized laser beam in the TEM$_{oo}$-Mode with a noise component of less than 0.5%, and thus are well suitable for being utilized with the LDI.

Diodes:

For the registration of a single signal or sometimes two simultaneous signals, the PIN-diodes from Hewlett Packard, type 5082-4207 were used. For more than two beams, the (linear) arrays from United Detector Technology, type PIN-SA60 was employed. PIN-diodes have linear characteristics over many orders of magnitude. They make high resolution in time in the ns-range possible. The high quantum efficiency for HeNe-laserlight of about 70% achieves signal currents in the mA-range for laser output of some mW, such that even the signals from very sensitive measurements can be sent directly to the internal oscilloscope amplifiers.

Wollaston Prisms:
In order to achieve beam separation distances in a wide range from 1/100 mm to some cm, a large collection of Wollaston prisms were available: quartz prisms with prism angles α = 10', 20', 1°, 2°, 4°, 8°, 10°, 20°, 30°, and calcite prisms with the angles α = 4° and 8°. The corresponding division angles ε and beam separation distances a are given by eqns. (1) and (2). The following constants are used at the laser wavelength λ = 6328 Å: $|n_{ex} - n_{or}|$ = 9.05·10^{-3} for quartz, and $|n_{ex} - n_{or}|$ = 0.169 for calcite. All Wollaston prisms were obtained from the company Jean Fichou, 30 Rue de la Garenne, Fresnes, France.

Lenses, Objectives:
For most arrangements, conventional lenses would have been sufficient. However, because of their antireflection coating, doublets from the Spindler & Hoyer company, Göttingen have been used almost exclusively. In the interferometer, focal lengths varied between 5 cm and 150 cm. For focussing or generating large light bundles, smaller focal lengths and microscopic objectives have been utilized.

For the optical arrangement with deflecting mirrors in fig. 19, interferometer quality objectives of high quality are necessary. For the registration of the signals from a temperature boundary layer shown in fig. 20 the interferometer was assembled with astro-objectives AS 80/1200 from the Zeiss company. It also can be used as Schlieren mirror pair.

Large laser light bundles as in fig. 25 and fig. 26 require interferometer objectives with corresponding large aperture. For these arrangements, objectives from Boyer, Saphir 1:1 4/50, 1:1 9/125 and 1:1 9/200 were available.

Polarizers:
Any polarizing filters from photo industry or from optical kits are useable.

λ/4-plates:
When accepting a small contrast decrease as a compromise, common λ/4-plates from kits, designed for medium lightwave range and fulfilling no special requirements will suffice in most instances. For optical arrangements with laser bundles of large diameter, λ/4-plates of high quality were manufactured of quartz by the Fichou company. They were tuned to a wavelength of λ = 6328 Å.

Test Section Windows:

The test section windows also do not require special optical quality. Only the arrangement with mirror deflection, fig. 19, requires interferometer quality windows.

Tripods, Optical Benches, Supports:
Due to the relative low sensitivity of a differential interferometer to vibrations the mechanical hardware does not have to fulfill special requirements as well. Tripods, optical benches and supports were supplied by the Spindler & Hoyer company. The rest of the mechanical parts, e.g. mounts, displacement drives and so on came from miscellaneous sources or were manufactured in the institute's machine shop.

Deflecting Mirror:
A magnetic coil vibrator with fluid damping from Siemens, type S 15000 T, served as deflecting mirror (fig. 19 and fig. 23), being able to follow frequencies up to about 10 kHz.

Pockels Cell:
The pockels cell in the optical arrangement in fig. 26 was the type EOM-401A from the Lasermetrics company.

Interference Filters:
Interference filters with bandpass width $\Delta\lambda$ between 10 Å and 30 Å were used.

Power Source:
Any battery can serve as a power source. The necessary currents are some mA at maximum.

Resistors:
Variable resistors in the range of 100 Ω and 100 kΩ were used as load resistors.

Signal Recording:
Since most measurements consisted of the recording of rapidly changing signals, the registration almost exclusively took place using oscilloscopes or fast digital recorders.

Literature

Differential Interferometer

[1] H. Oertel,
A Differential Interferometer for Measurements in the Hypersonic Shock Tube.
Ein Differentialinterferometer für Messungen im Hyperschallstoßrohr.
(Un interféromètre différentiel pour les mesures dans le tube de choc hypersonique.)
ISL - T 17/61   (1961).

[2] G. Smeets,
Differential Interferometer for Observation and Measurements of Boundary Layers.
Differentialinterferometer zur Beobachtung und Ausmessung von Grenzschichten.
(Interféromètre différentiel pour l ' observation et la mesure de couches limites.)
ISL - T 25/64   (1964).

[3] G. Smeets,
Differential Interferometer with large beam separation. Data Reduction of the Interferograms.
Differentialinterferometer mit großer Strahltrennung. Auswertung der Interferogramme.
(Interféromètre différentiel à faisceaux fortement séparés. Dépouillement des interférogrammes.)
ISL - T 41/68   (1968).

Laser-Differential Interferometer

[4] G. Smeets,
4-Beam Laser Interferometer for Measurement of Transient Weak Phase Objects.
4-Strahl-Laser-Interferometer zur Messung an schnellveränderlichen schwachen Phasenobjekten.
(Interféromètre laser à 4 faisceaux pour la mesure des objets de phase faibles présentant des variations rapides.)
ISL - T 21/70   (1970).

[5] G. Smeets,
Laser Interferometer for Measurement of Transient Weak Phase Objects.
Laser-Interferometer zur Messung an schnellveränderlichen schwachen Phasenobjekten.
Optics Communications, Vol. 2, Nr. 1 (1970).

[6] G. Smeets,
     A High Sensitive Laser Interferometer for Transient Phase Objects.
     Shock Tube Research, Proc. 8th Int. Shock Tube Symposium, London (1971).

[7] G. Smeets, A George,
     Gas-Dynamic Investigations in the Shock Tube with a Highly Sensitive Laser-
     Interferometer.
     Gasdynamische Untersuchungen im Stossrohr mit einem hochempfindlichen Laser-
     Interferometer.
     *(Etudes en dynamique des gaz effectueés au tube à choc à l'aide d'un interféromètre
     laser très sensible.)*
     ISL - 14/71 (1971)

[8] G. Smeets,
     Laser-Interferometer for High Sensitive Measurements on Transient Phase Objects.
     IEEE Transactions AES, Vol.8, No. 2 (1971)

[9] G. Smeets,
     Laser-Interferometer with Large, Focussed Light Bundles for Local Measurements.
     Laser-Interferometer mit großen, fokussierten Lichtbündeln für lokale Messungen.
     *(Interféromètre à larges faisceaux focalisés pour des mesures localisées au voisinage du
     foyer.)*
     ISL - N 11/73   (1971)

Gas-Dynamic Investigations with the LDI

[10] G. Smeets,
     Measurement of the Growth of the Laminar or Turbulent Boundary Layer on a Hollow
     Cylinder in a Shock Tube with Constant Cross Section.
     *Messung der Bildung der laminaren oder turbulenten Grenzschicht an einem
     Hohlzylinder im Stoßrohr konstanten Querschnitts.*
     ISL - NI 72/4   (1972)

[11] G. Smeets,
     Flow in the ISL Hypersonic Shock Tube. Measured Air Densities behind a Nozzle with
Knife Edge Exit.
     *Strömung im Hyperschallstoßrohr des ISL. Gemessene Luftdichten hinter einer Düse mit
     scharfem Düsenmund.*
     ISL - NI 72/19   (1972)

29

[12] A. George,
   Density Profile Measurements behind the shock wave of a Pointed Cone with Half-Angle 12.5°.
   Profils mesurés de la masse volumique dans l'onde de tête d'un cône pointu de demi-angle 12.5°.
   ISL - NI 72/27   (1972)

[13] H. Oertel,
   Investigations of the Turbulent Boundary Layer on a Flat Plate in Supersonic High Temperature Air Flow.
   Untersuchungen der turbulenten Plattengrenzschicht in Überschallströmungen heißer Luft.
   ISL - NI 73/8   (1973)

[14] G. Smeets,
   Investigation of Shock Boundary Layers with a Laser Interferometer.
   Proc. 8th Int. Shock Tube Symposium Stanford (1973)

[15] G. Smeets,
   Experimental Determination of the Thermal Conductivity of Air and Air-Water Mixtures in the Temperature Range 2000 K $\leq$ T $\leq$ 7000 K.
   Experimentelle Bestimmung der Wärmeleitfähigkeit von Luft und Luft-Wasser-Gemischen im Temperaturbereich 2000 K $\leq$ T $\leq$ 7000 K.
   ISL-Report pending.

[16] G. Smeets,
   Experimental Investigation into Turbulent Boundary Layers in Supersonic Flow of Hot, Partially Dissociated Air.
   Experimentelle Untersuchungen an turbulenten Grenzschichten in Überschallströmungen heißer, teildissoziierter Luft.
   ISL-Report pending.

[17] G. Smeets,
   Utilization of a Laser-Differential Interferometer for the Determination of Local Fluctuations and the Average Density Profile in a Turbulent Free Flow.
   Verwendung eines Laser-Differential-Interferometers zur Bestimmung lokaler Schwankungsgrößen sowie des mittleren Dichteprofils in einem turbulenten Freistrahl.
   ISL-Report pending.

Figures

CW-Laser

λ/4-plate

Wollaston Prism

Lenses

Windows

Phase

Object

Wollaston Prism

Lens

Polarization Filter

Photo Diode

α

ε

a

variable

f

variable

f

Imaging

Fig. 1

Fig. 2

Signal Recording

Fig. 3

M = 9 Flow

Fig. 4

$1{,}1 \cdot 10^{-3} \rho_N$

$100\,\mu s$
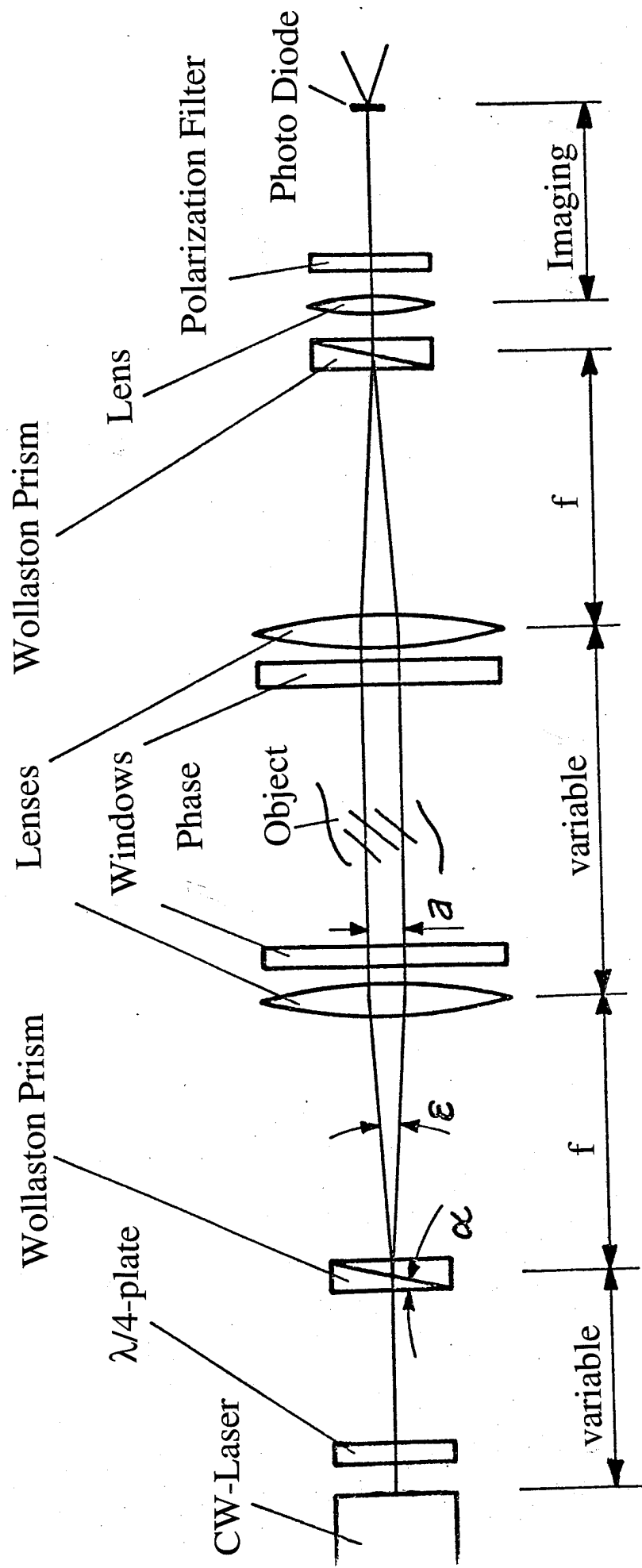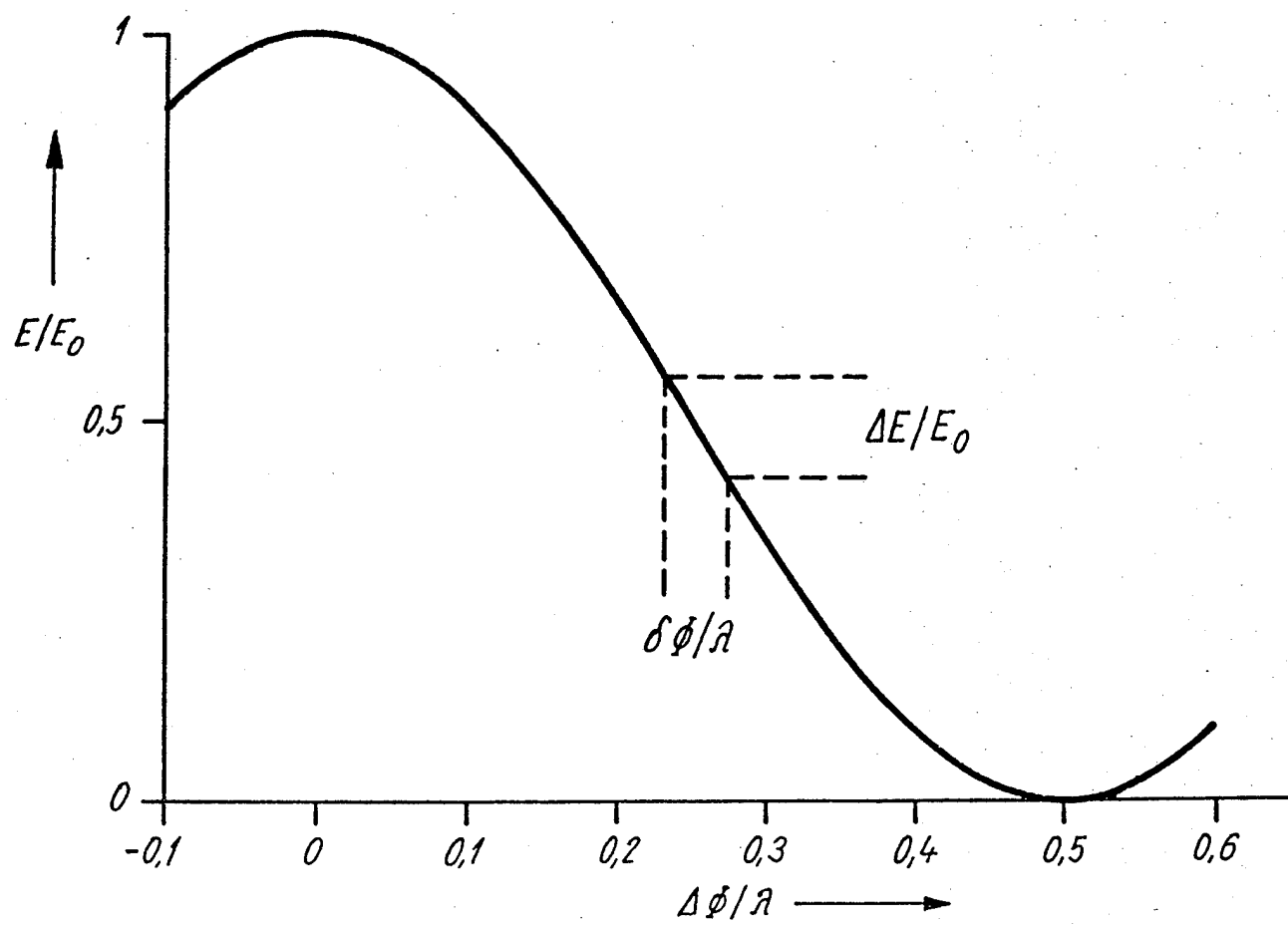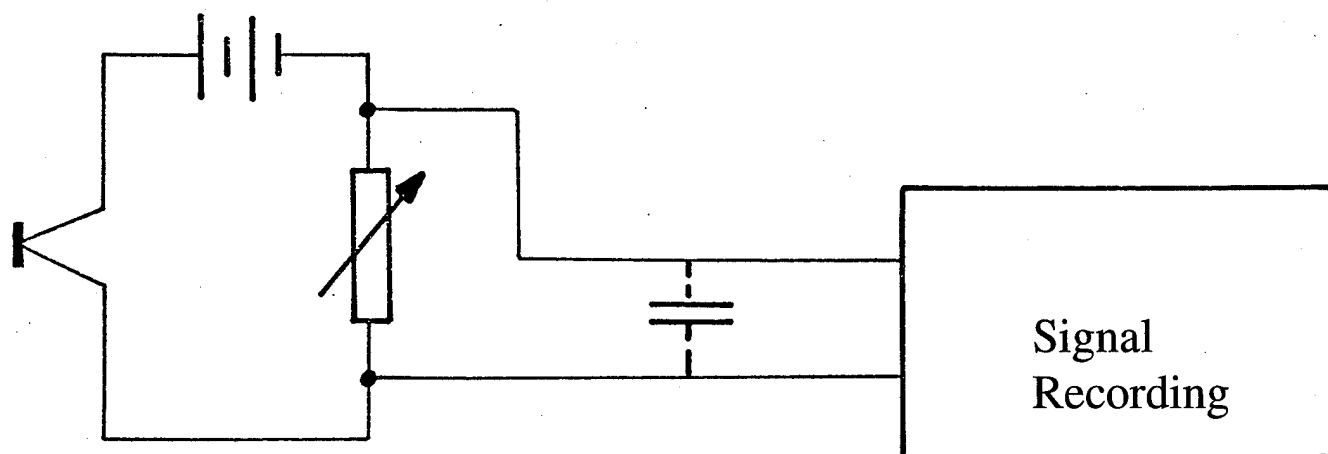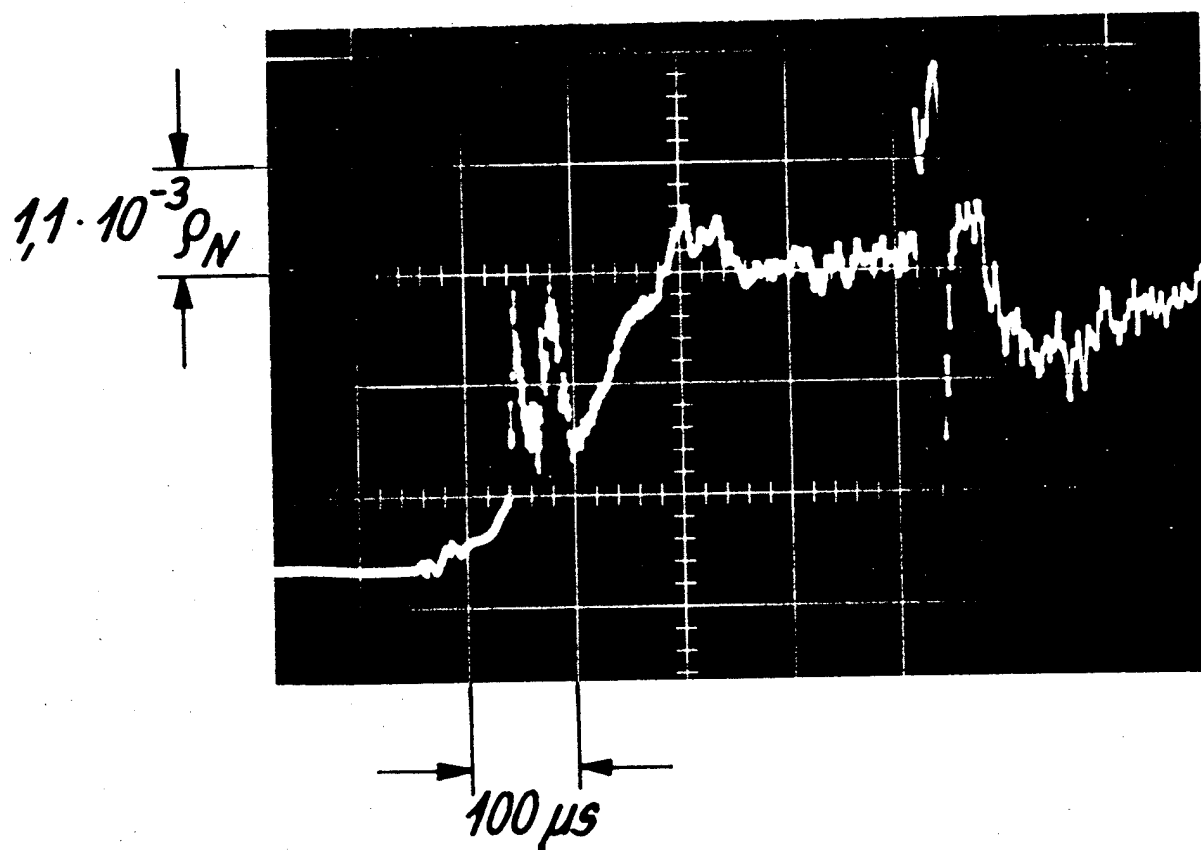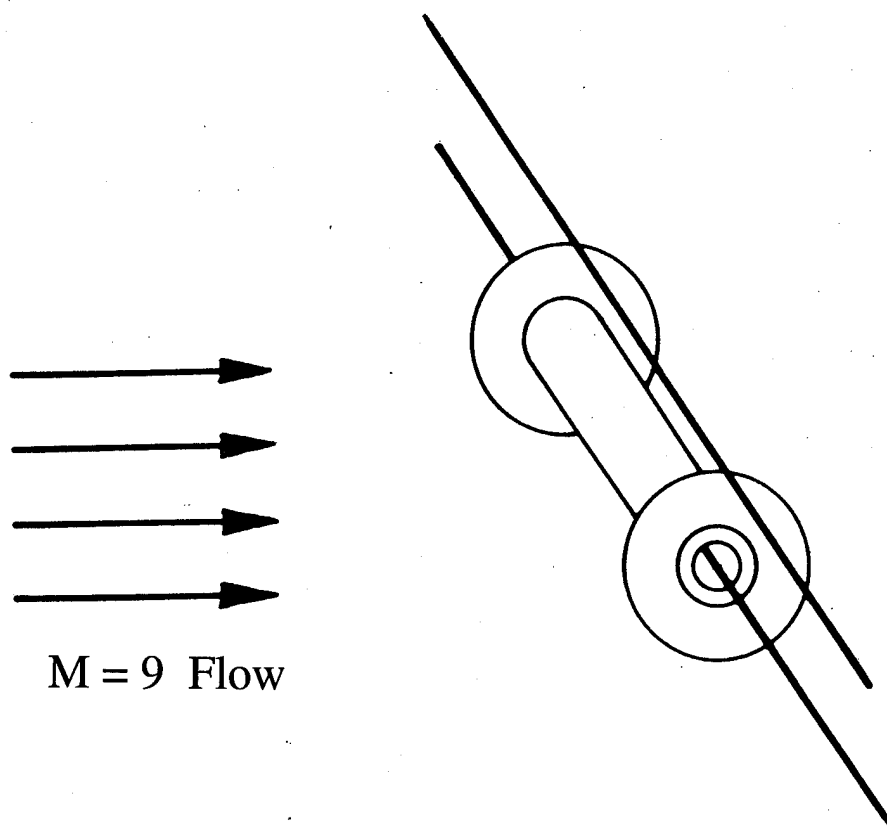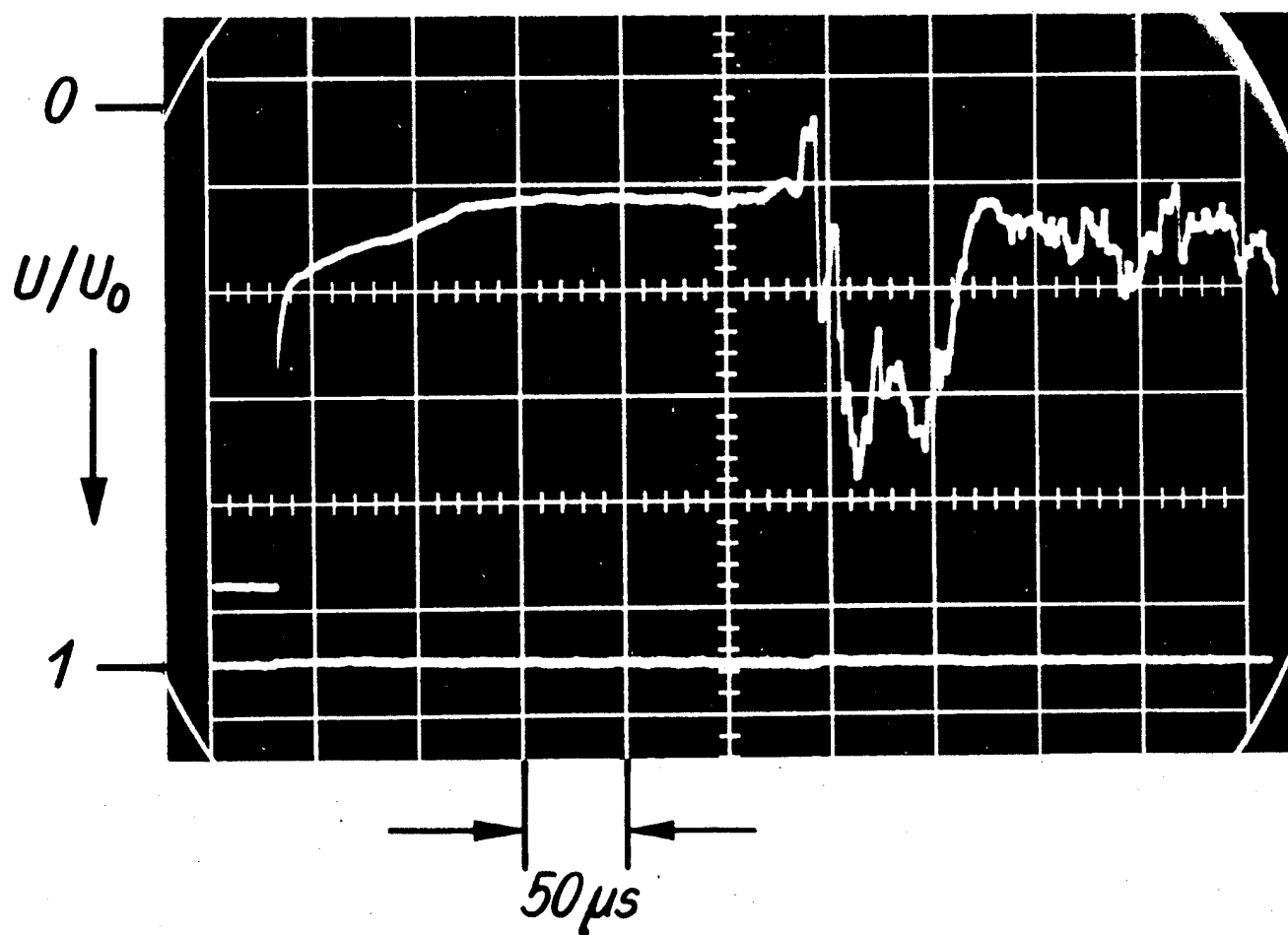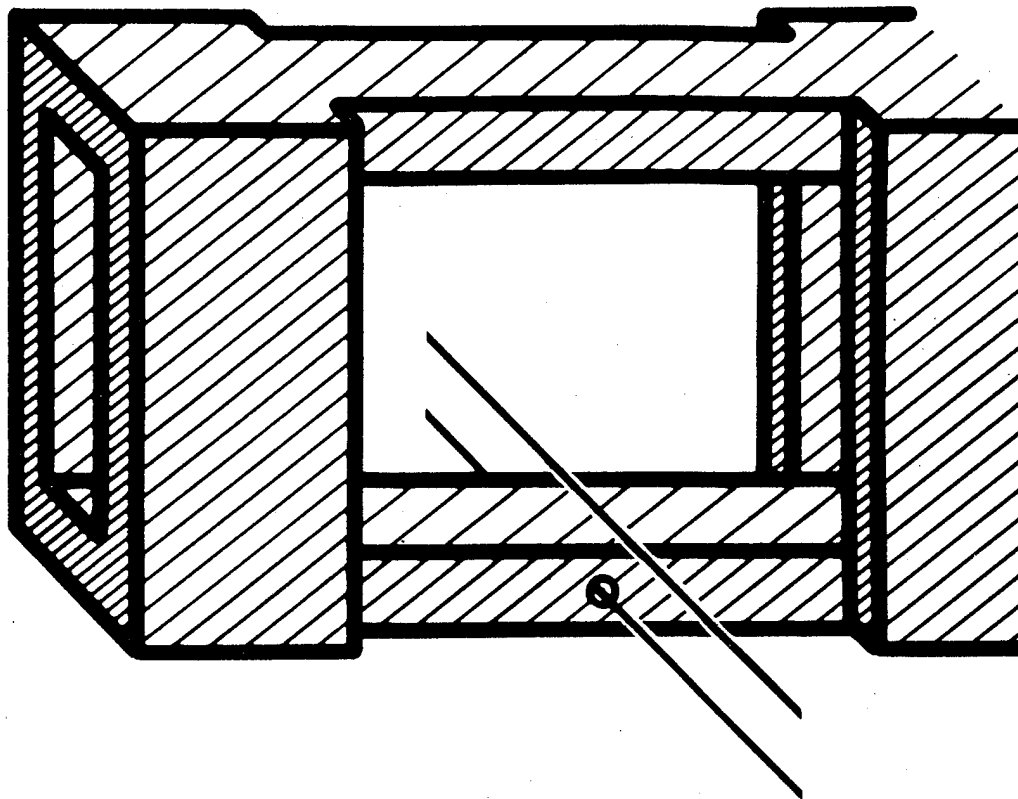
Air $p_1 = 1$ Torr $M_s = 9.5$ Fig. 5

Fig 6

λ/4-plate

Wollaston Prism

Photo Diodes

Signal Recording

Fig. 7

Wollaston Prism

$\lambda/4$-plate

Lens

Fig. 8

Cover

Fig. 9

Fig. 10

Lenses

D

f

ϑ

$\hat{d}$

41

Fig. 11

Shock Wave →

100 Å

0,5 μs
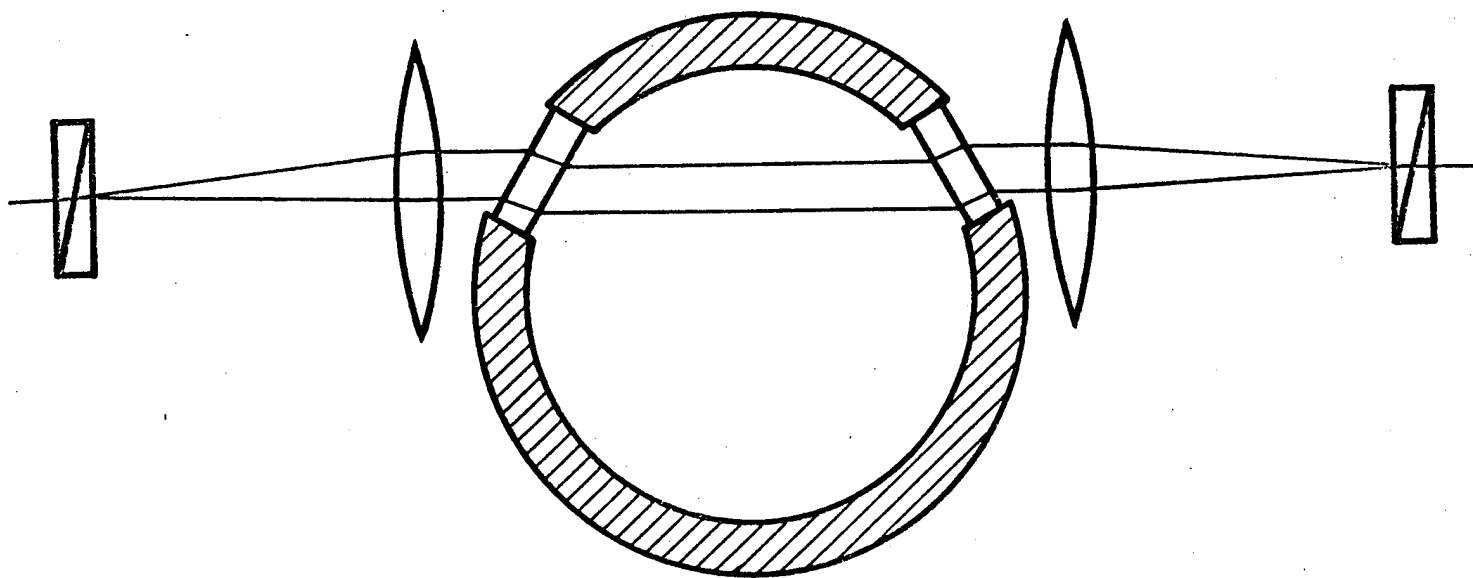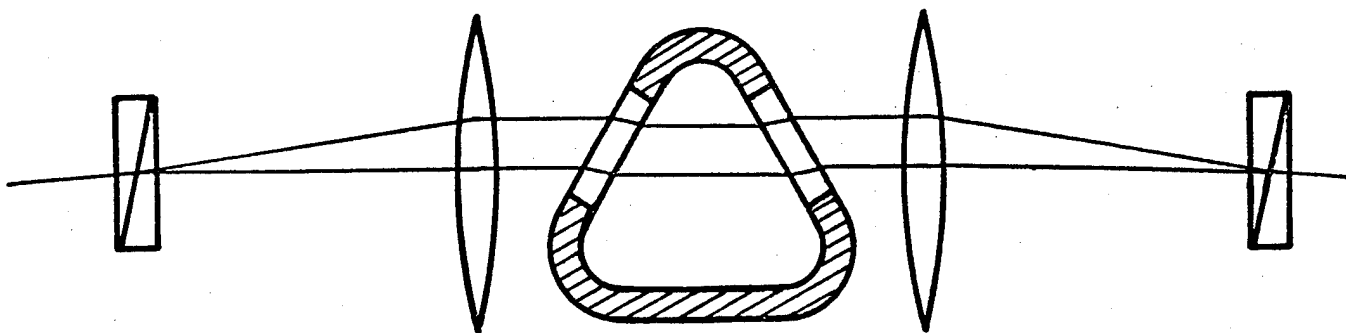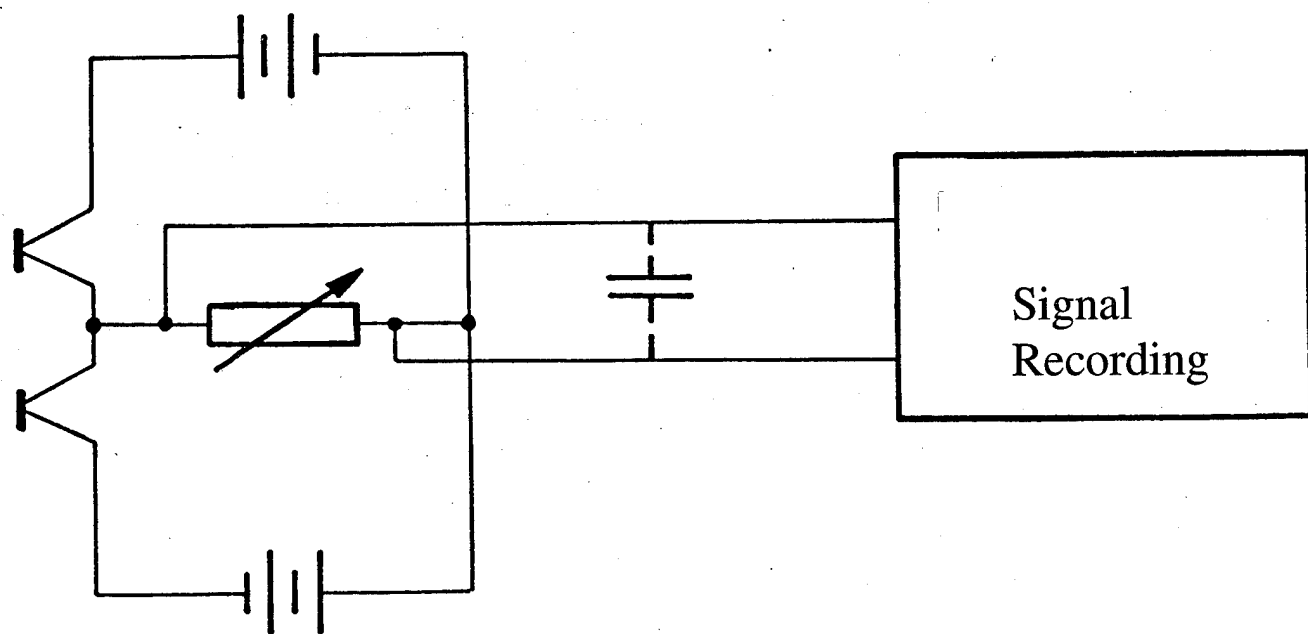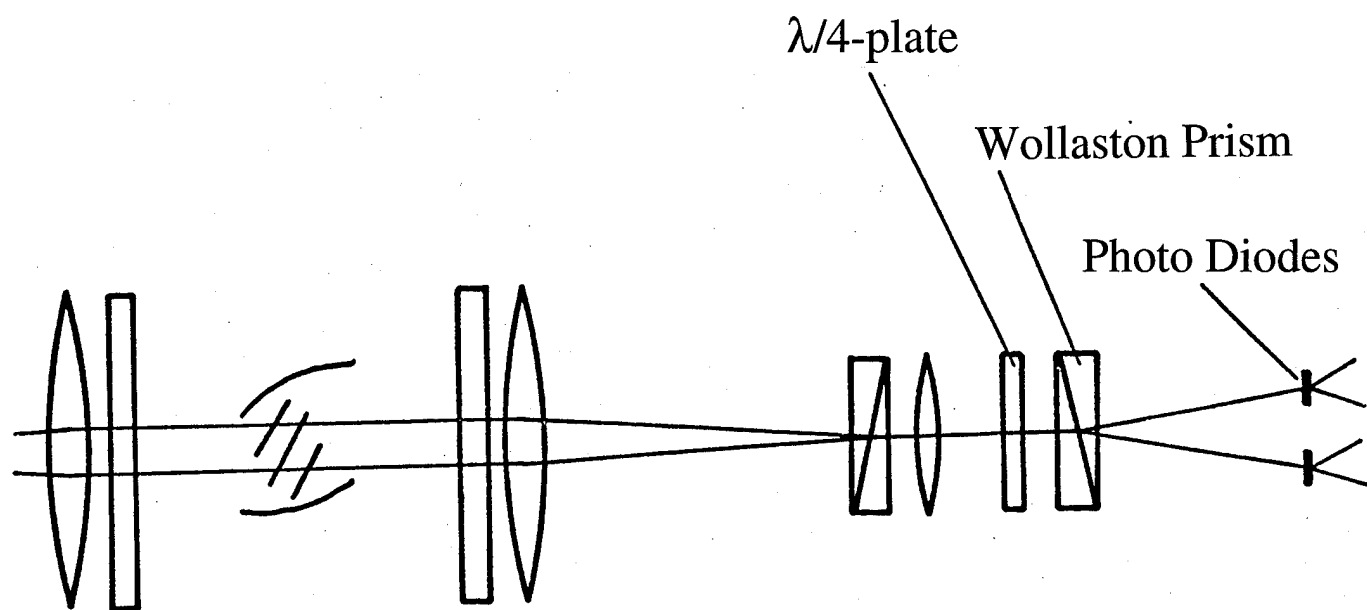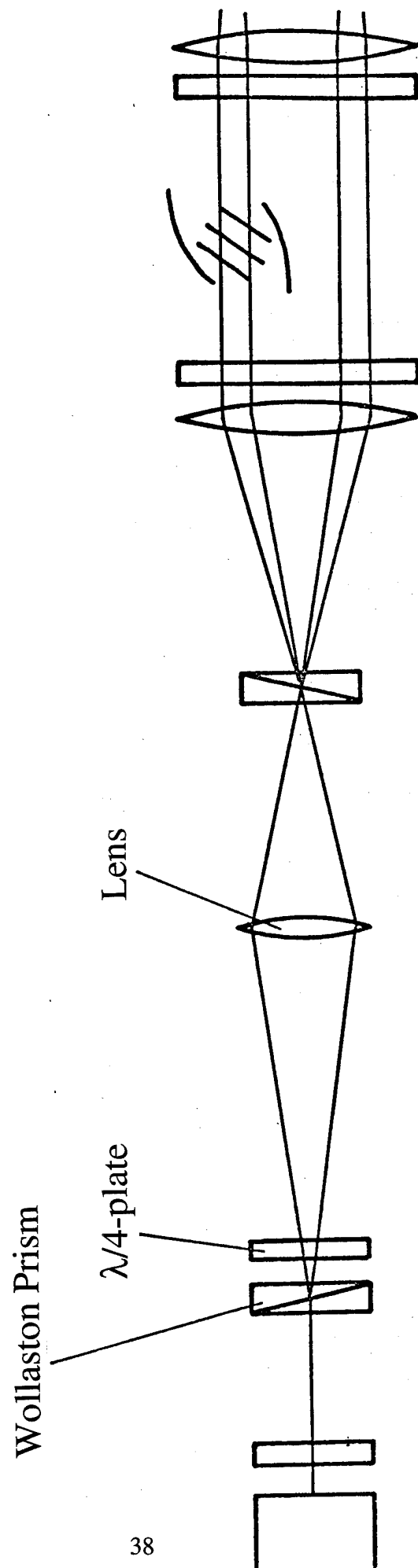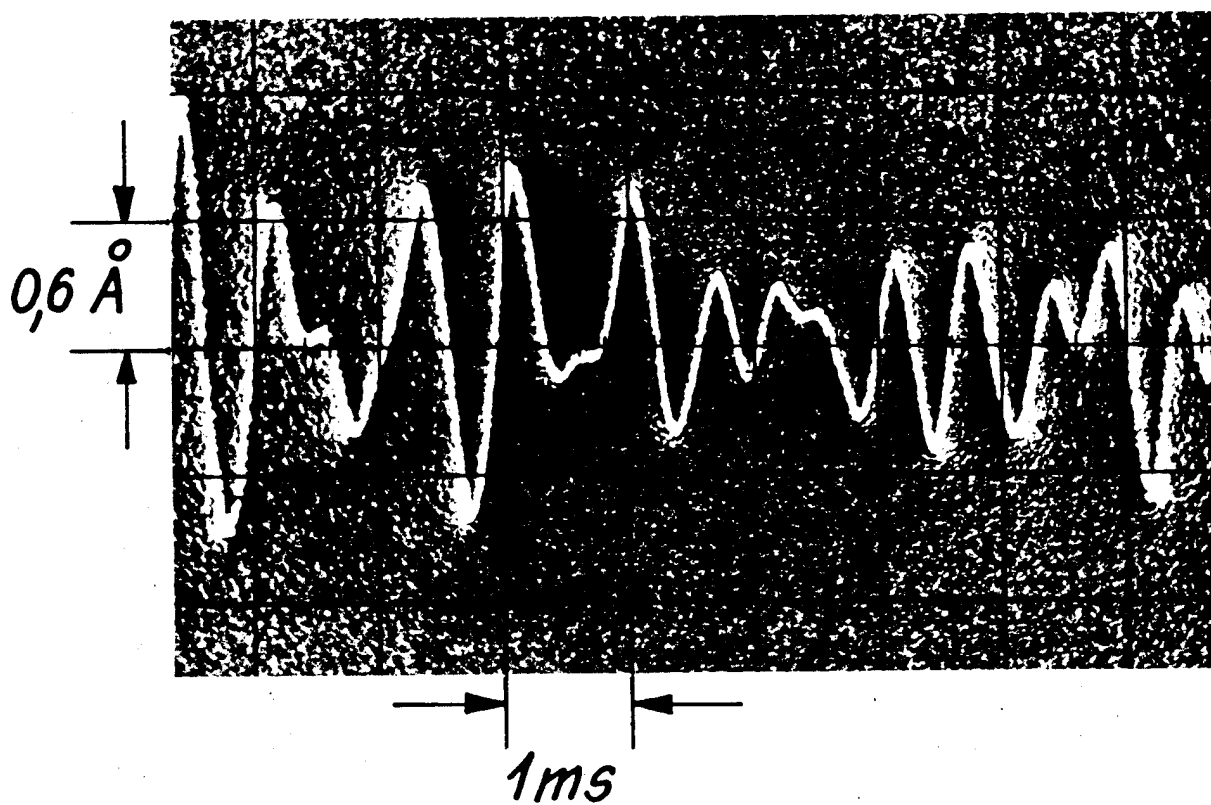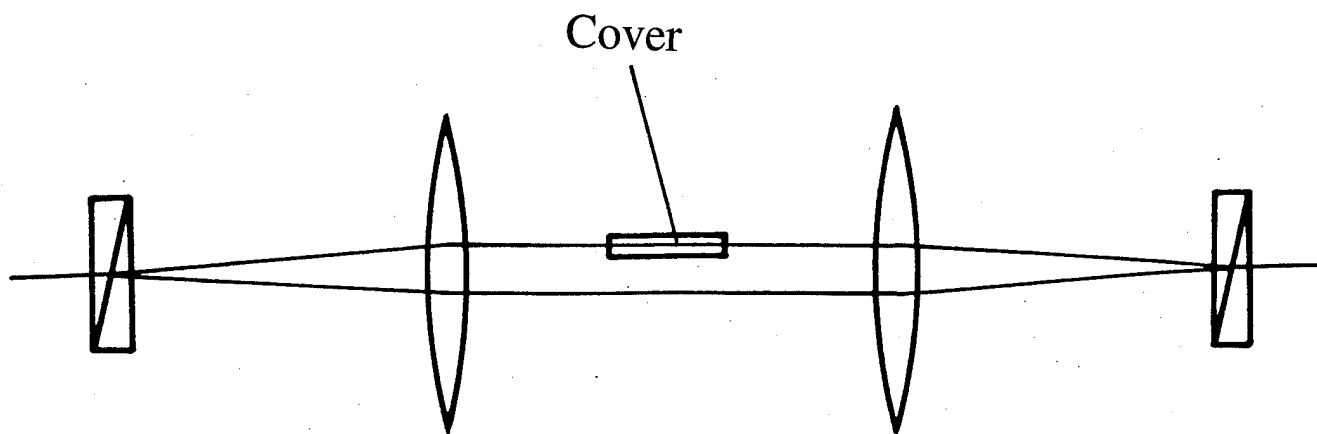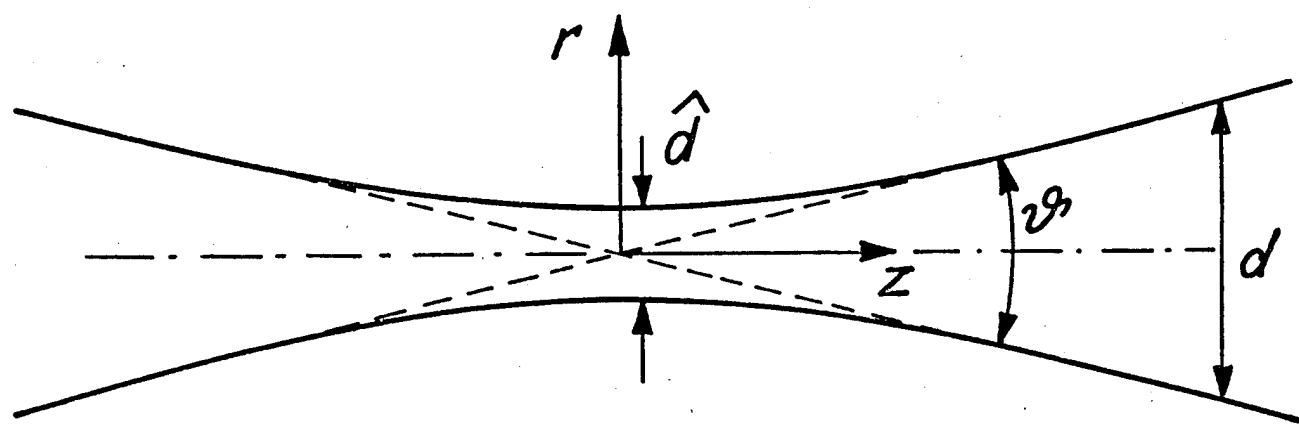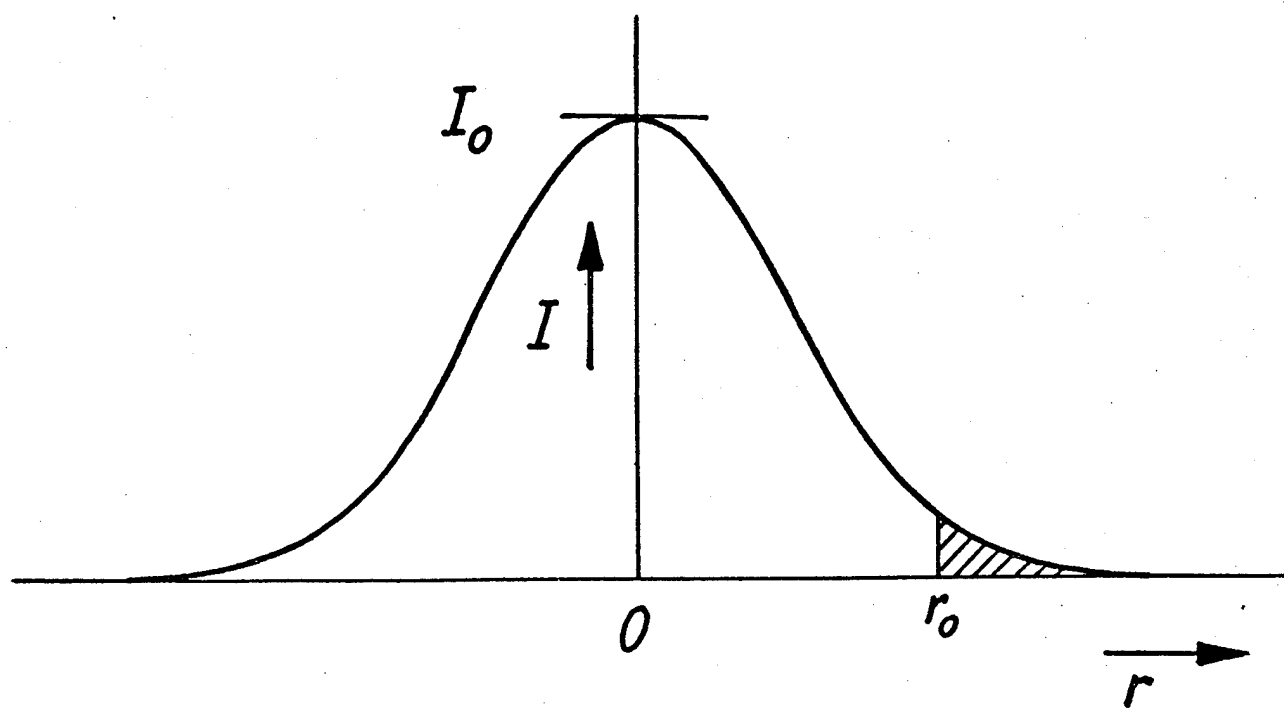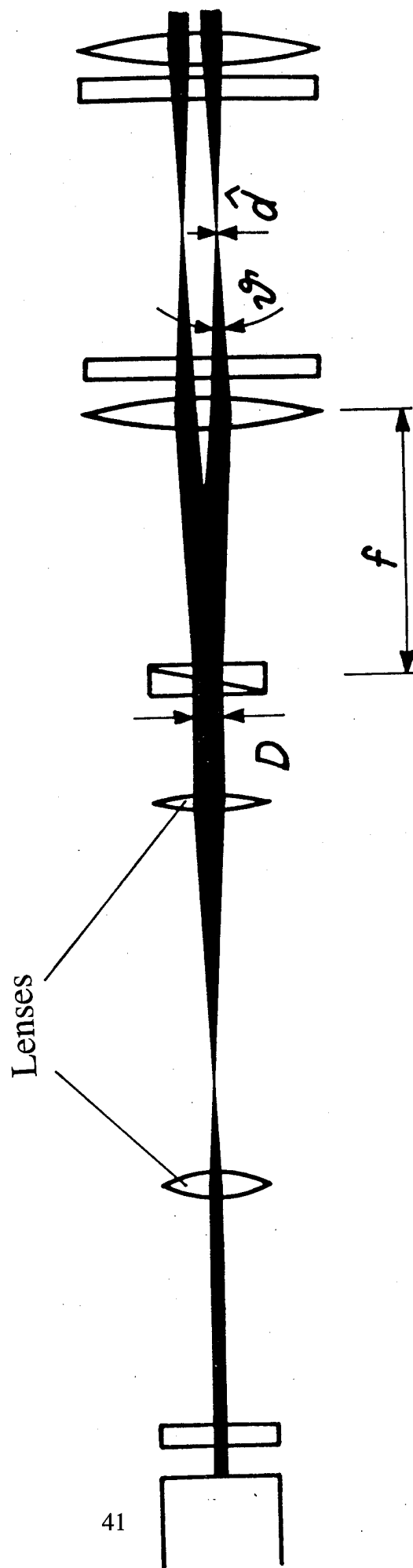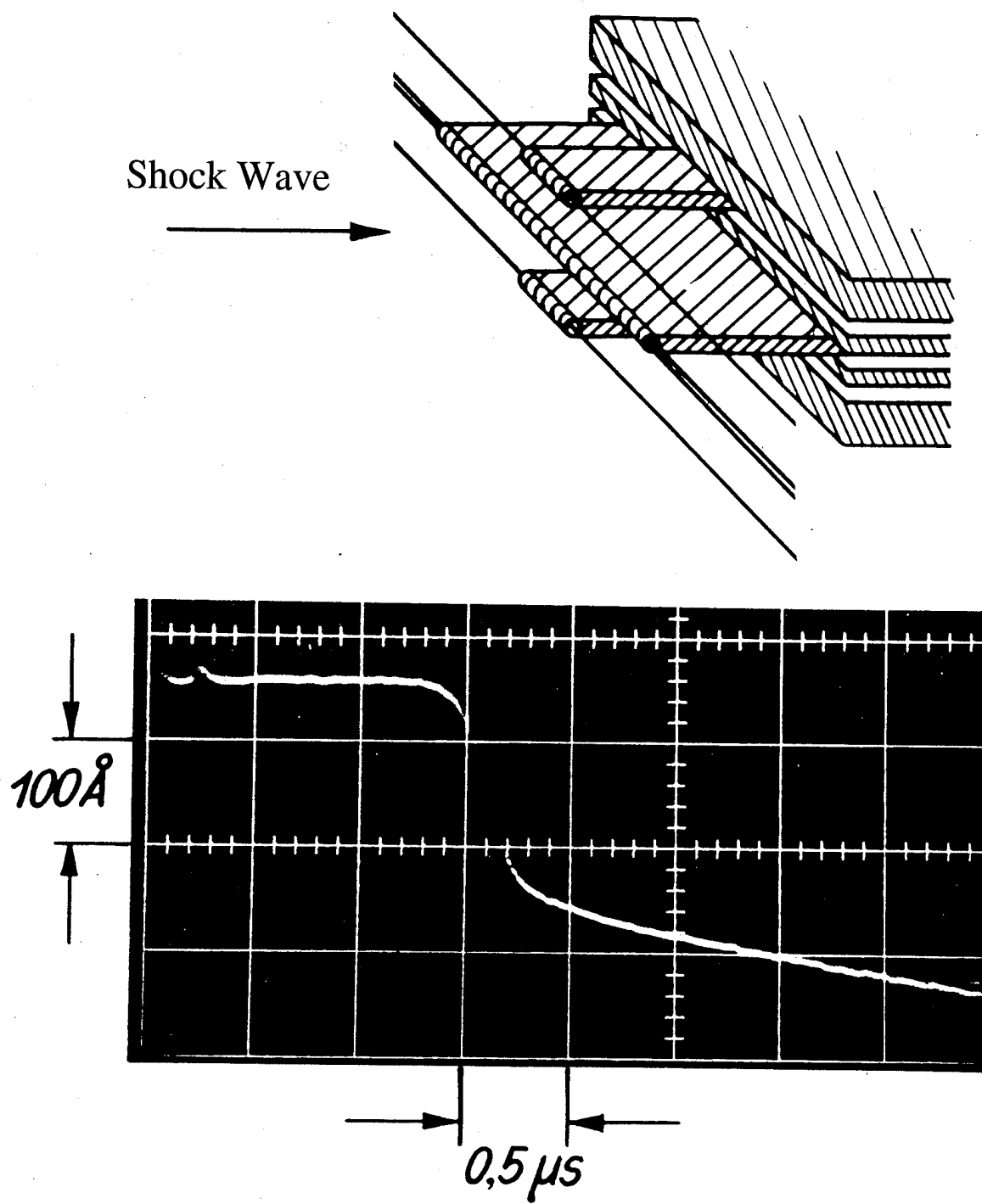
Air   p₁ = 0.2 Torr $M_s = 13.3$ Fig. 12

Wollaston Prisms

λ/4-plates

Lens

Lens

Diode Array

Fig 13

43

Signal
Recording

Fig. 14

$Re = 8 \cdot 10^4$

$\rho_2 = 2 \cdot 10^{-2} \rho_N$

$u_2 = 2650\,m/s$

	y/mm
1	0,03
2	0,17
3	0,34
4	0,47
5	0,64
6	0,78
7	0,95
8	1,09

Fig. 15

$Re = 1{,}6 \cdot 10^{6}$

$\rho_2 = 0{,}5\, \rho_N$

$u_2 = 1150\ \text{m/s}$

10 cm

5 4 3 2 1

y / mm

1 – 2   0,025 – 0,150

2 – 3   0,150 – 0,275

3 – 4   0,275 – 0,400

4 – 5   0,400 – 0,525

20μs

Fig. 16

8 Rays

$M = 9$

$\rho = 3 \cdot 10^{-3} \, \rho_N$

$125 \, \overset{\circ}{A}$

$100 \, \mu s$

47

Fig. 17

Air

$p_1 = 0.2$ Torr
$U_s = 1570$ m/s

x/mm

4
                                               1,2

3
                                               1,0

2

1
                                               0,8

                                               0,6

$50 \mu s$

48   Fig. 18

Lens

Deflecting Mirror

Lens

Lens

Fig. 19

49

Temperature Boundary Layer

Heated Plate

1 cm

Gradient Signal

200 μs

1 cm

Integrated Signal

200 μs

Fig. 20

Fig. 21

Cover   Pressure Waves

Loudspeaker

Gradient Signal

Integrated Signal

Fig. 22

50 μs

Fig. 23

Turbulence

Parabolic Reflector

Fig. 24

2nd Interferometer

Deflecting Mirror

Mirror

λ/4-plate

Fig. 25

55

Polarization Filter

Pockels cell

Fig. 26

56

to
Charge Amplifier

C

R

Short Duration
Signal
Recording

Fig. 27

Turbulent

Window Boundary Layer

Objective

Fig. 28

58

Turbulence

Micro Objective

Fig. 29

Free Flow

Light Stop

Koester Prism

CW-Laser

Wollaston Prisms

λ/4-plates

Diode Array

Fig. 30

60

Fig. 31

Turbulent
Window Boundary Layer

Turbulent
Model Boundary Layer

Partial Mirror

Polarization
Filter

Fig. 32

1 Å

2 μs

Fig. 33

Interference Filter

Light Stops

Fig. 34

Splitting Mirror

Fig. 35

65

	Field of Interest	Type of Measurement, Investigation	Set-up in Fig.	Literature
1.	Calibration of Flows in Gas-Dynamic Arrangements	Experimental Determination of ρ(t)	4,5,6	[6] [7] [8] [11]
		Experimental Determination of a(t), u(t)	11	
2.	Gas Dynamics of Compressible Flow	Density Distribution in Flows around Models	11,13,17,19,20	[6] [7] [8] [12]
		Density Distribution in Free Flow	11,13,19,20	[17]
3.	Boundary Layers	Density Profiles of Shock Layers	11,13,15,16,25	[6][7][8][10][14]
		Density Profiles of steady Boundary Layers (Shock Tunnel, Wind Tunnel)	11,13,15,16,19, 20,25	[10][13][14][16]
		Density Profiles of the End Wall Boundary Layer in the Shock Tunnel (λ-Measurement)	11,13,18	[6] [7] [8] [15]
		Density Profiles of Temperature Boundary Layers of Heated Surfaces	11,13,19,20	
		Mixing Region between two Gas Flows	11,13,19,20	
		Diffusion Boundary Layers	11,13,19,20	
4.	Gas Kinetics (Kinetics of Reactions)	Shock Front Profiles (Translatory and Rotatory Relaxation)	11,12	[7] [8]
		Relaxation (of Oscillation, Chem. Reactions, Ionisation)	5,6	[6] [7] [8]
		Determination of Refractive Indices	5,6	
5.	Turbulence	Turbulence Structure of Boundary Layers	13,28,29,30,32	[9]
		Turbulence Structure of Free Flows	13,24,29,30,31	[9] [17]
		Free Turbulence	13,29,30	
		Turbulent Mixing of Gases	13,29,30	
6.	Acoustics	Profiles of Weak Shocks (Bang, Dispersed Shock Waves)	7,9,23	
		Propagation of Sound Waves, i.e. Ultrasonic Waves (Reflection, Focussing)	13,23,24,33	
		Transmission of Loudspeakers (Microphones)	22,23	

Figure 36

66